Screening for substrate tolerant *Geobacillus pallidus* RAPc8 nitrile hydratases

Moses Clive Masisange Mketsu

A thesis submitted in partial fulfillment of the requirements for the degree of Magister Scientae in the Department of Biotechnology, University of the Western Cape.

Supervisor: Prof D.A. Cowan
Co-supervisor: Dr I.M. Tuffin
November 2009

Abstract

Screening for substrate tolerant *Geobacillus pallidus* RAPc8 nitrile hydratases

Moses Clive Masisange Mketsu

MSc thesis, Department of Biotechnology, University of the Western Cape.

Nitrile hydratases (NHases) from microorganisms are used for the industrial biotransformation of nitriles to amides. Industrial bioconversion of nitriles is attractive over chemical conversion, because of no by-product formation, stereo-selectivity and mild reaction conditions of temperature and pH required, where harsh conditions may be detrimental to certain chemical functionalities. The thermostable cobalt-type *Geobacillus pallidus* RAPc8 NHase was previously cloned into a pET21a vector under a *lac* promoter and expressed in *Escherichia coli.* The enzyme was shown to be active on aliphatic and heteroaromatic nitriles but no activity on homoaromatic nitriles was detected. Homoaromatic specificity was engineered into the enzyme with the construction of the βF52GβF55L mutant. Furthermore it was shown that the enzyme is substrate inhibited by 3-cyanopyridine (heteroaromatic), which is undesirable for industrial biotransformation.

In this study *G. pallidus* RAPc8 NHase mutants were screened for reduced substrate inhibition compared to the wild type enzyme. Wild type and mutant enzymes were expressed and purified using hydrophobic interaction chromatography. Amidase coupled enzyme stop assays were conducted using 3-cyanopyridine as a substrate, whereas continuous enzyme kinetics were conducted using acrylonitrile as a substrate.

The Michaelis-Menten and Briggs-Haldane model were fitted to the 3-cyanopyridine and acrylonitrile hydration enzyme kinetic data. Only the Briggs-Haldane model fitted to the 3-cyanopyridine data as all the enzymes were strongly inhibited by 3-cyanopyridine. The wild type

(K_i = 22.67mM) and βF52GβF55L mutant (K_i = 26.76mM) were substrate inhibited to a similar extent, while the αW124G mutant (K_i = 0.45mM) had a more than 50-fold increase in substrate inhibition compared to the wild type. Preliminary experiments using crude extracts of the βW76G mutant showed a 46-fold reduction in 3-cyanopyridine substrate inhibition compared to the partially purified wild type enzyme. In contrast the acrylonitrile kinetic data fitted well to both the Michaelis-Menten model and the Briggs-Haldane model. Similar substrate inhibition constants (K_i) were obtained for the wild type (K_i = 2338mM) and βF52GβF55L (K_i = 2243mM) mutant, indicating low substrate inhibition by acrylonitrile. A significant difference was observed between the wild type and αW124G mutant (K_i = 441mM). The αW124G mutant had the highest substrate inhibition by acrylonitrile with only the Briggs-Haldane model fitting to the kinetic data.

Cavity analysis of mutant NHase models showed an increase in cavity dimensions compared to the wild type model. However, there was no direct correlation between cavity size and substrate inhibition. Acrylonitrile docked the best, with the highest energy and shortest nitrile nitrogen to cobalt metal ion distance in a catalytically active orientation in the wild type NHase model. 3-cyanopyridine docked the best in the βF52GβF55LβW76G mutant model, suggesting that the mutant could potentially be tolerant to high concentrations of 3-cyanopyridine just as the wild type is tolerant to high concentrations of acrylonitrile.

November 2009

Declaration

I declare that *Screening for substrate tolerant Geobacillus pallidus RAPc8 nitrile hydratases* is my own work, that it has not been submitted before for any degree or examination in any other university, and that all the sources I have used or quoted have been indicated and acknowledged as complete references.

Moses Clive Masisange Mketsu November 2009

Signed: . . . . . .

Acknowledgements

Praise be to God for giving me the ability and strength to complete this study. I would like to thank my family, my father, mother, siblings and the Church. Thanks to my supervisor Prof Don Cowan for allowing me to conduct this study and co-supervisors Dr Marla Tuffin and Mr Lonnie van Zyl and the whole of IMBM for their support. Finally I would like to thank the National Research Foundation (NRF) for their financial support.

Table of contents

List of tables and figures

Abbreviations

Å	angstrom
Abs	absorbance
ASP	ammonium sulphate precipitation
BSA	bovine serum albumin
Da	Dalton
g	gravity or gram
hrs	hours
HIC	hydrophobic interaction chromatography
IPTG	Isopropyl -D-1-thiogalactopyranoside
kb	kilo base pairs
kDa	kilodalton
K_i	substrate inhibition constant
K_M	Michaelis-Menten constant
mM	milli molar
min	minute
MVD	Molegro Virtual Docker
NHase	Nitrile Hydratase
Ω	Ohm
PAGE	polyacrylamide gel electrophoresis
PCR	polymerase chain reaction
PDB	Protein Data Bank
r.m.s.d	root mean square deviation
SDS	sodium dodecyl sulphate
sec	seconds
sp.	species

v/v volume per volume

V_{max} maximum velocity (rate of enzyme-catalysed reaction at infinite substrate concentration)

w/v weight per volume

µM micromolar

Chapter 1: Literature review

1.1 Introduction

Nitriles, the organic cyanides (R≡N) are found throughout nature in the plant, animal and microbial kingdoms (Legras, 1990). In plants nitriles are known to act as growth hormones. C14, C15 and C16 alkyl nitriles promote the growth of stem sections in *Pisum sativam* (Stowe and Hudson, 1969). Indole-3-acetonitrile is known to act as a plant growth hormone (Woodward and Bartel, 2005). Nitriles are also used in defence against predators. In plants when cyanogenic glycosides undergo enzymatic hydrolysis, cyanohydric acid is released which can link with metal ions, which are functional groups of certain important enzyme, thereby inactivating those enzymes (Francisco *et al.,* 2000). The larva of the mountain ash sawfly *Pristiphora geniculata* is known to secrete mandelonitrile in defence against predators (Duffield *et al.,* 1990). In streptomyces, nitriles are known to act as antibiotics (Vino and Lokesh, 2008). However, their role in bacteria is still uncertain, though evidence suggests that they are used in energy production (see section 1.2).

Enzymes known to be involved in nitrile bioconversion include the NHases (Nagasawa and Yamada, 1990), nitrilases (Dhilon *et al.,* 199) and isonitrile hydratases (Goda *et al.,* 2001). The most studied of these classes of enzymes is the NHases, owing to their application as industrial biocatalysts (Yamada and Kobayashi, 1996). NHases are metalloenzymes containing either a non-heme ferric iron or non-corrinoid cobalt acting as Lewis acids and are therefore designated as Fe-NHases and Co-NHases respectively. NHases catalyse the hydration of nitriles to amides, which can then be hydrolysed by amidases to carboxylic acids (Wang, 2005). This chapter seeks to review the recent literature in the field of NHase enzymes.

1.2 Biological role of NHases

NHases are part of a group of enzymes involved in the aldoxime-nitrile pathway (Asano and Kato, 1998). In plants, aldoximes are derived from amino acids in a reaction catalysed by microsomal peroxidases and are known to be intermediates in the biosynthesis of compounds such as indoleacetic acid, cyanogenic glycosides and glucosinolates (Bak *et al.,* 2001; Halkier and Gershenzon, 2006).

The source of aldoximes in bacteria and its biological role (Fig 1.1) has only recently become evident (Kato *et al.,* 2007; Hashimoto *et al.,* 2005; Kobayashi *et al.,* 2005). Aldoximes in bacteria, as in plants, are derived from amino acids. In a study using *Bacillus* sp. OxB-1, L-phenylalanine was converted to N-hydroxy-l-phenylalanine (L-NHP), though the enzyme(s), which catalyses the conversion has/have not been isolated (Kato *et al.,* 2007). L-NHP was then converted to Z-phenylacetaldoxime (Z-PAOx) in a reaction presumably catalysed by N-hydroxy-l-phenylalanine decarboxylase/oxidase. Z-PAOx was dehydrated to phenylacetonitrile by phenylacetaldoxime dehydratase (Oxd) (Asano and Kato, 1998). Hydrolysis of phenylacetonitrile by the nitrile degrading enzymes NHase/amidase and nitrilase leads to phenylacetate formation. In a study using *P. chlororaphis* B23, acyl-CoA synthetase (AcsA) activity was detected in conjunction with aldoxime dehydratase, NHase, and amidase activity (Hashimoto *et al.,* 2005). Acyl-CoA forms when a thioester bond forms between a carboxylic acids (acyl) reacts with CoA (thiol) with water removal in a reaction catalyzed by acyl-CoA synthetase (AcsA) (Hashimoto *et al.,* 2005). Acyl-CoA is used in many biochemical reactions including energy production in the Krebs cycle and in the synthesis of the neurotransmitter acetylcholine (Colletier *et al*., 2006). This suggests that the aldoxime-nitrile pathway forms part of a pathway for energy metabolism of amino acids.

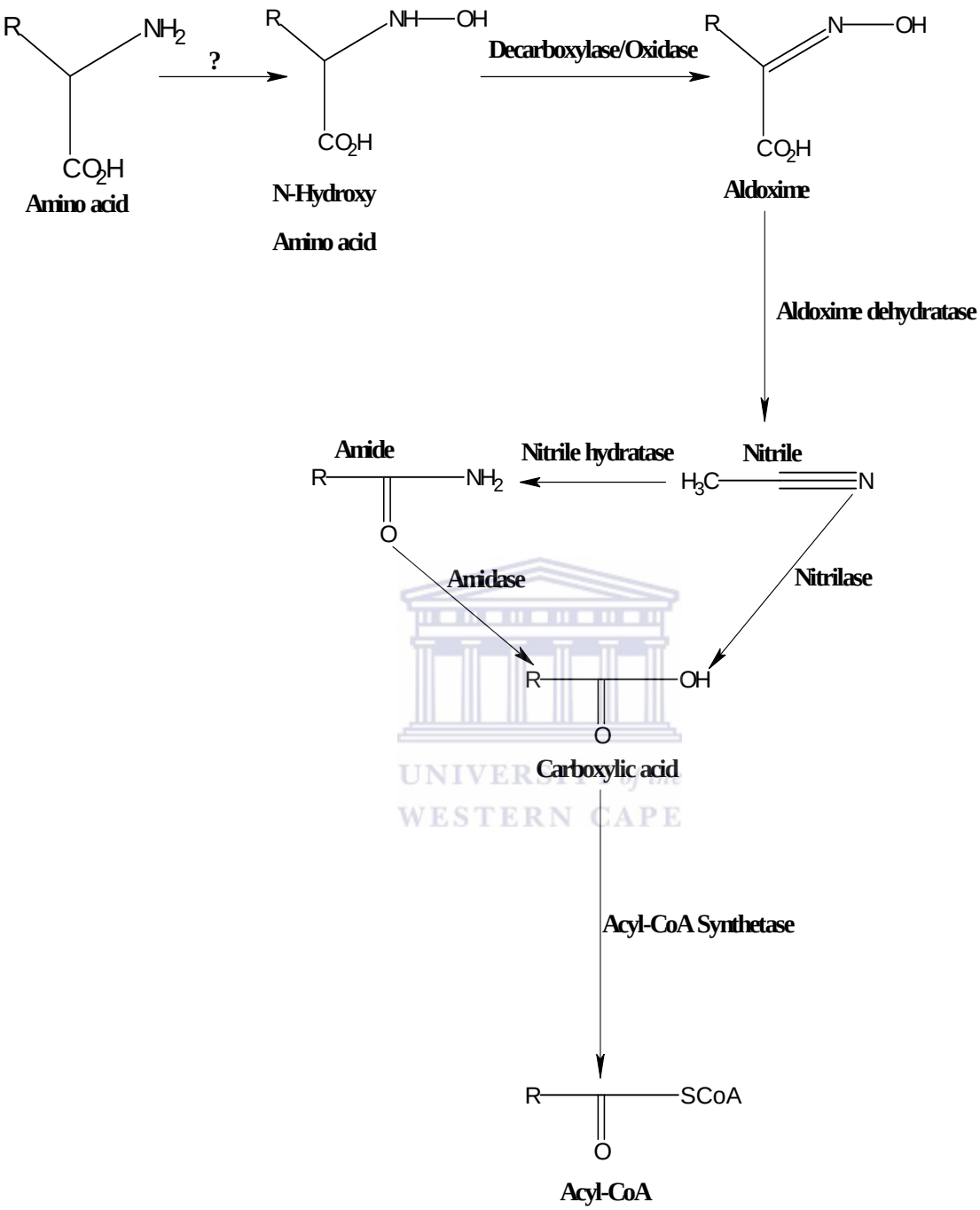

Figure 1.1: The complete aldoxime-nitrile pathway (Redrawn from Kato and Asano, 2003; Kato et al., 2007).

1.3 NHase selection, expression and screening

The preferred method for isolating nitrile metabolising microorganisms is selection, where microorganisms are grown using nitriles as the sole carbon and/or nitrogen source (for review see Martinkova *et al.*, 2007). *G. pallidus* RAPc8 (formerly *Bacillus pallidus* RAPc8) was isolated using acetonitrile as the sole nitrogen and carbon source (Pereira *et al.*, 1998). The desired substrate specificity in the enzyme usually dictates the choice of substrate used in the enrichment procedure. When 2-phenylpropionitrile was used as the sole nitrogen source, an enantioselective NHase from *A. tumefaciens* d3 was isolated which converted the nitriles to the corresponding S-amides (Stolz *et al*., 1997). An acidotolerant nitrile-hydrolyzing yeast *Exophiala oligosperma* R1 was isolated at pH 4 using glucose as the sole carbon source and phenylacetonitrile as the sole nitrogen source (Rustler and Stolz, 2007).

While culture dependent methods have enabled the isolation of many NHases, this method poses limitations to the discovery of NHases with novel activities. Estimates indicate that between 1% and 10% of the total microbial diversity has been cultured, with the remaining majority termed unculturables because the conditions for culturing these microorganisms have not been determined (Cowan, 2000). The use of PCR metagenomic methods has enabled the isolation of NHases from unculturable microorganisms with novel substrate specificities (Brandao *et al.*, 2003). Though the NHase isolated were novel they still had much similarity to know NHase sequences showing that PCR dependent metagenomic techniques are limited in the gene diversity they can isolate.

In native microorganisms expression of the NHases is constitutive (Takashima *et al.*, 1998; Kim and Oriel, 2000) for some microorganisms and inducible (Komeda *et al.*, 1996; Nagasawa *et al.*, 1991) for others. The use of suboptimal growth temperature using *E. coli* as an expression host is known to enhance the solubility of recombinant proteins (Hannig and Makrides, 1998).

Expression of the *Bacillus* sp BR449 NHase at suboptimal growth temperature in the presence of $CoCl_2$ yielded active soluble enzyme, whereas prior expression at above optimal temperature yielded inactive enzyme (Kim and Oriel, 2000). Heat treatment of the NHase apoenzyme in the presence of 5μM $CoCl_2$ resulted in greater specific activity of the *G. pallidus* RAPc8 NHase (Tsekoa, 2005) and *Bacillus* sp BR449 NHase (Kim and Oriel, 2000). Co-expression of thermostable NHase from *G. pallidus* RAPc8 with a p14K auxiliary protein enhanced the specific activity of the enzyme significantly (Cameron *et al*., 2005). P14K is suspected to participate in facilitating proper folding of the NHase α-subunit and the incorporation of the cobalt ion into the active site cleft (see section 1.4.1). The co-expression of an iron type NHase from *Comamonas testosteroni* with GroES and GroEL resulted in higher levels of soluble protein expressed, while expression in the absence of the chaperones resulted in lower levels of protein insolubly expressed (Stevens *et al*., 2002).

An ideal method for NHase activity screening is the direct continuous method. Direct continuous methods are rapid and provide easily reproducible data. The spectral absorbance for amides (products of NHase hydration) is in the UV region, acrylamide has an absorbance at 225nm, benzonitrile at 242nm and 3-cyanopyridine at 235nm (Tsekoa, 2005). H-NMR spectroscopy has also been used in the detection of NHase activity owing to the chemical shift of 2 parts per million between nitrile and amides (Jallageas *et al*., 1979). Coupled continuous or stopped methods can also been used in screening for NHase activity. Conductivity (Reisinger *et al*., 2004) and pH (Banerjee *et al*., 2003) change can be used as a method for activity testing in an amidase coupled reaction. A discontinuous coupled stop assay (ammonia assay) has been used in determining NHase activity owing to the easy accessibility of the instruments used to conduct the assay (Pereira *et al*., 1998).

1.4 Molecular analysis

1.4.1 *G. pallidus* RAPc8 NHase operon gene structure

The NHase gene cluster form *G. pallidus* RAPc8 is 5.9kb long and contains eight structural genes (Fig 1.2) (Cameron *et al.,* 2005). The arrangement starts with an amidase, followed by the NHase β, α subunit respectively, p14K (122 amino acid accessory protein), 2Fe-2S homologue class of ferredoxins and three proteins homologues to cbiM, cbiN, cbiQ and cbiO genes coding for proteins responsible for cobalt uptake in the *Salmonella typhimurium* LT2 cobalamin (vitamin B12) biosynthesis pathway (Rodionov *et al.,* 2006).

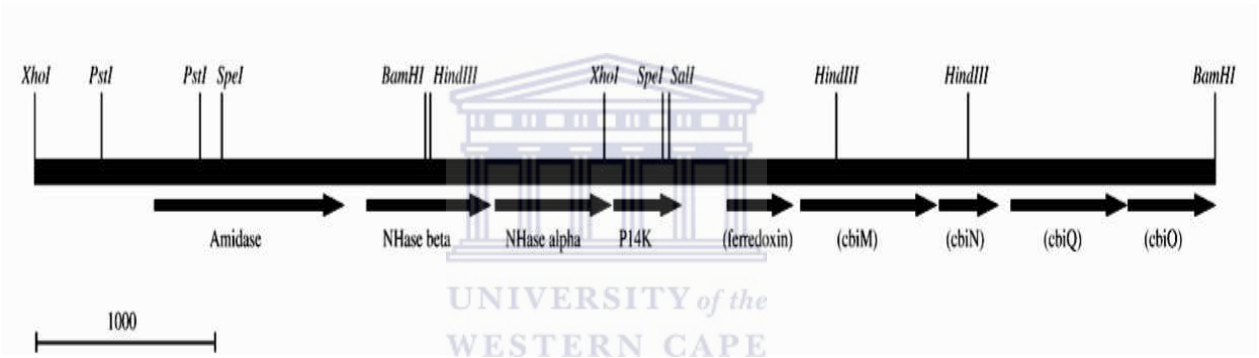

Figure 1.2: *G. pallidus* RAPc8 NHase gene cluster (Cameron *et al*., 2005).

The NHase from this gene cluster is a cobalt type and the p14k accessory protein is suspected to be important for proper folding of the α subunit and incorporation of the cobalt ion, which is required for catalytic activity (Cameron *et al.,* 2005). Recombinant expression of the NHase gene in the presence of the p14K gene resulted in a 32-fold increase in the activity of the expressed enzyme compared to expression in the absence of the p14K gene. However, Recombinant expression of the *Bacillus* sp. BR449 NHase does not require co-expression with p12K (a p14K homolog) (Kim and Oriel, 2000). A p15K auxiliary protein required for the functional expression of a recombinant thiocyanate Hydrolase has also been reported (Arakawa *et al.,* 2007).

Four tentative mechanisms have been proposed for the formation of a native catalytically active NHase (Fig 1.3). Mechanism D seems to be the most likely because it has been shown that incorporation of cobalt into the enzyme is not passive (Cameron *et al.*, 2005). In this mechanism the α subunit is stabilized by the binding of a cobalt ion through an interaction with p14K. Binding of the β subunit leads to the displacement of the p14K protein to form the native holoenzyme.

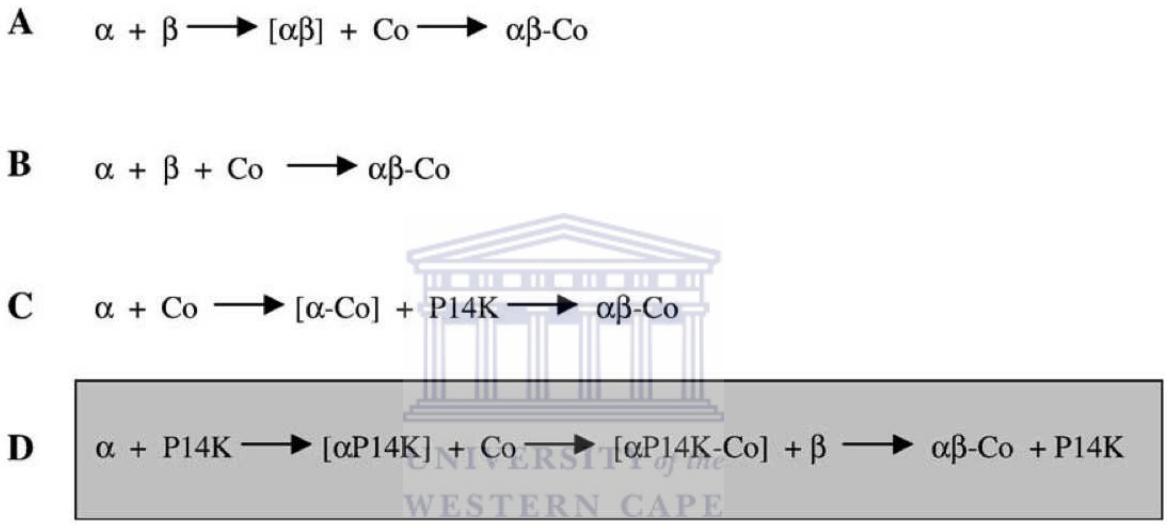

Figure 1.3: Tentative mechanisms for the formation of NHase holoenzyme: A) αβ apoenzyme forms followed by cofactor (Co) binding. B) α, β and Co bind simultaneously C) Co binds to folded α subunit, then the β subunit binds to form holoenzyme (D) α subunit interacts with P14K allowing the binding of Co, P14K is then displaced by the β subunit (Cameron *et al.*, 2005).

1.4.2 Functional characteristics: pH and temperature

Mesophilic and thermophilic NHases have similar pH profiles, which have a sharp fall off in enzymatic activity towards low pH values (Cramp and Cowan, 1999). Most NHases have optimal enzymatic activity around the neutral pH, with a mildly acidic pH lower limit (pH 6) (Nagasawa *et al*., 1987) and a basic (pH 10) (Takashima *et al*., 1998) upper limit. Though the maximum activity range is narrow, *Rhodococcus* sp. YH3-3 NHase is stable over a wide pH range between pH 2.5 and pH 11 (Kato *et al.*, 1999).

NHases are described as either thermophilic or mesophilic based on their temperature optima. To date there is no description of a hyperthermophilic or psychrophilic NHase in the literature. The temperature optima range for thermophilic NHase is between 40°C and 60°C (Takashima *et al*., 1998; Pereira *et al*., 1998) and between 10°C and 35°C (Tani *et al*., 1989; Langdahl *et al*., 1996) for the mesophilic counterparts. All thermostable NHases have a cobalt ion prosthetic group in the catalytic centre, whereas the majority of mesophilic NHases have an iron ion prosthetic group in the catalytic centre (Table 1.1). The contributing factor for the enhanced thermostability of thermophilic NHase compared to the mesophilic counterparts is unclear. The additional α-β (α36-α49/β111-β125) helical interactions was suggested to be the contributing factor for the enhanced thermostability of Co-type NHases (Miyanaga *et al*., 2001). Sequence comparison between mesophilic and thermophilic Co-type NHases revealed the same structural motif, suggesting that the motif is only a characteristic of Co-type NHases and does not contribute to enhanced thermostability (Cowan *et al*., 2003). Thermostability of NHases can be enhanced using cofactors. N-butyric acid has been shown to enhance the thermostability of an Fe-type NHase by preventing further oxidation of the post-translationally modified cysteine residues in the active cleft (Odaka *et al*., 2001). Crude extracts of *G. pallidus* RAPc8 NHase have substantially higher thermostability than the purified enzyme, indicating that the cellular environment provides additional stability for the enzyme (Cowan *et al*., 1998).

Table 1.1: pH and temperature optima of thermophilic and mesophilic NHases.

Organism	pH optima	Temperature optima (°C)	Prosthetic group	Reference
Thermophilic				
Bacillus pallidus RAPc8	7	60	Co	Pereira *et al.*, 1998
Bacillus pallidus Dac521	7-7.5	50	Co	Cramp and Cowan, 1999
Bacillus sp. BR449	7.5	55	Co	Kim and Oriel, 2000
Pseudonocardia thermophila JCM 3095	Un	60	Co	Yamaki *et al.*, 1997
Rhodococcus sp. YH3-3	7	40-60	Un	Kato *et al.*, 1999a
Mesophilic				
Rhodococcus rhodochrous J1	6-8.5	35	Co	Nagasawa *et al.*, 1991
Rhodococcus erythropolis ATCC 25544	7.5	30	Un	Yeom *et al.*, 2007
Rhodococcus sp. R312	7-8.5	35	Fe	Nagasawa *et al.*, 1986
Corynebacterium sp. C5	8-8.5	10-40	Fe	Tani *et al.*, 1989
Agrobacterium tumefacies d3	7	40	Un	Bauer *et al.*, 1998

Un denotes undetermined.

1.4.3 Substrate specificity

The low molecular mass NHase (L-NHase) from *Rhodococcus rhodochrous* was shown to be specific for aliphatic nitrile methacrylonitrile (Wieser *et al*., 1998). Thermophilic *Bacillus* strains are known for aliphatic (Cramp and Cowan, 1999) and dinitrile (Pereira *et al*., 1998) (Takashima *et al*., 1998) specificity. The NHase from *Rhodococcus equi* A4 has stereoselectivity for the S-enantiomer of racemic 2-(2-, 4-methoxyphe-nyl) propionitrile, 2(4chlorophenyl) propionitrile and 2-(6-methoxynaphthyl) propionitrile (naproxennitrile) (Prepechalová *et al*., 2000). The NHase from *Pseudomonas putida* NRRL-18668 also exhibits greater stereospecificity for 2(S)-(4′-chorophenyl)-3-methylbutyronitrile than the (R)-enantiomer (Payne *et al*., 1997). Table 1.2 shows the substrate specificities of different microbial species harbouring NHases.

Table 1.2: Substrate specificities of NHases.

Organism	Substrate specificity	Reference
Bacillus pallidus RAPc8	Cyclic, dinitriles and aliphatics.	Pereira *et al.,* 1998
Bacillus pallidus Dac521	Aliphatics	Cramp and Cowan, 1999
Bacillus smithii SC- J05-1	Aliphatics and dinitriles	Takashima *et al.,* 1998
Rhodococcus rhodochrous J1 L and H-NHase	Aliphatics and aromatics	Wieser *et al.,* 1998
Rhodococcus sp. N-774	Aliphatic	Endo and Watanabe, 1989
Corynebacterium sp. C5	Cyclic, dinitriles and aliphatics.	Tani *et al.,* 1989
Rhodococcus. Erythropolis BL1	Aromatics, dinitriles and aliphatics.	Langdahl *et al.,* 1996
Rhodococcus sp. YH3-3	Aliphatics, dinitriles and aromatics.	Kato *et al.,* 1999
Pseudomonas putida NRRL-18668	Aliphatics, dinitriles and aromatics.	Fallon *et al.,* 1996

1.4.4 Description of *G. pallidus* RAPc8 NHase structure

The NHase from *G. pallidus* RAPc8 is a 110kDa 2α2β heterotetramer (Pereira *et al.*, 1998) in the native form, although the crystal structure reveals an αβ heterodimer in the asymmetric unit (Tsekoa, 2005). Two active sites, which comprise of the *claw setting motif* are located at the α-β interface of each αβ heterodimer (Fig 1.4). The *claw setting motif* forms part of a conserved sequence element (CXYCSC) in both the Co and the Fe type NHases (Stevens *et al.*, 2003), residues (116-121) on the α-subunit of *G. pallidus* RAPc8 NHase.

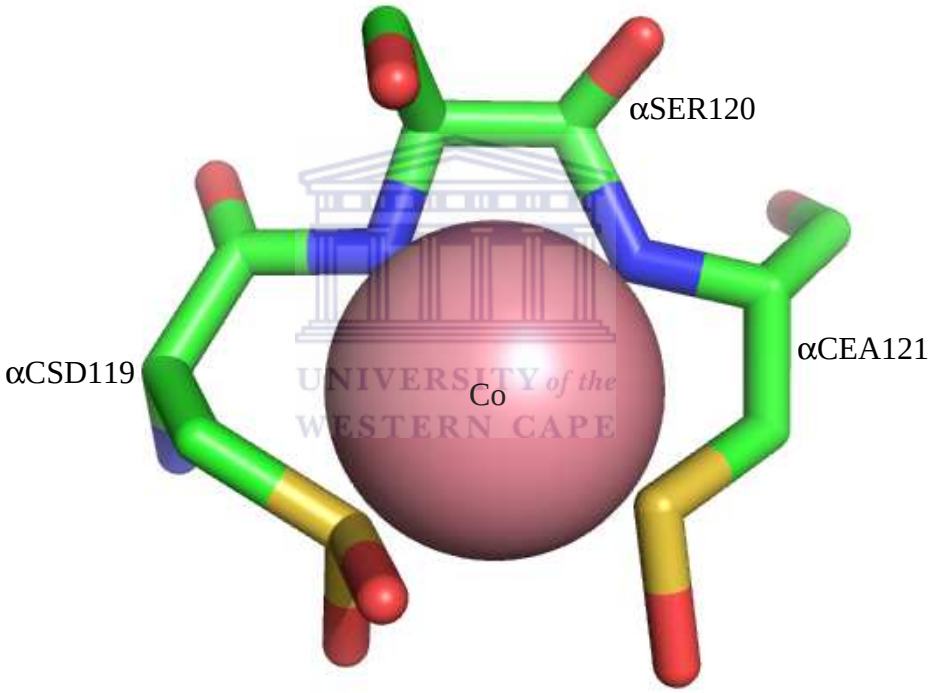

Figure 1.4: The *claw setting motif* of *G. pallidus* RAPc8 NHase. αCSD119 (cystein sulphinic acid 119), αSER120 (serine 120), αCEA121 (cystein sulphenic acid 121) and Co (cobalt).

The α subunit is made up of twelve α helixes and four β strands, with three of the α helixes protruding from the globular domain (Fig 1.5). The β subunit is comprised of two domains, the N-terminal (α-helix) domain and the C-terminal (β-sheet) domain (Fig 1.6). The N-terminal domain starts with a long loop connected to a short α helix, followed by a region consisting of seven α-helices. The C-terminal domain starts with two short α- helices and a β-strands respectively, followed by four anti parallel β-sheets at the C-terminal extremity. The topology of *G. pallidus* RAPc8 NHase is similar to that of *Rhodococcus* sp. R312 (Huang *et al.*, 1997) and possibly all NHases have a similar topology, resulting in a conserved fold amongst NHases (see section 1.5.6).

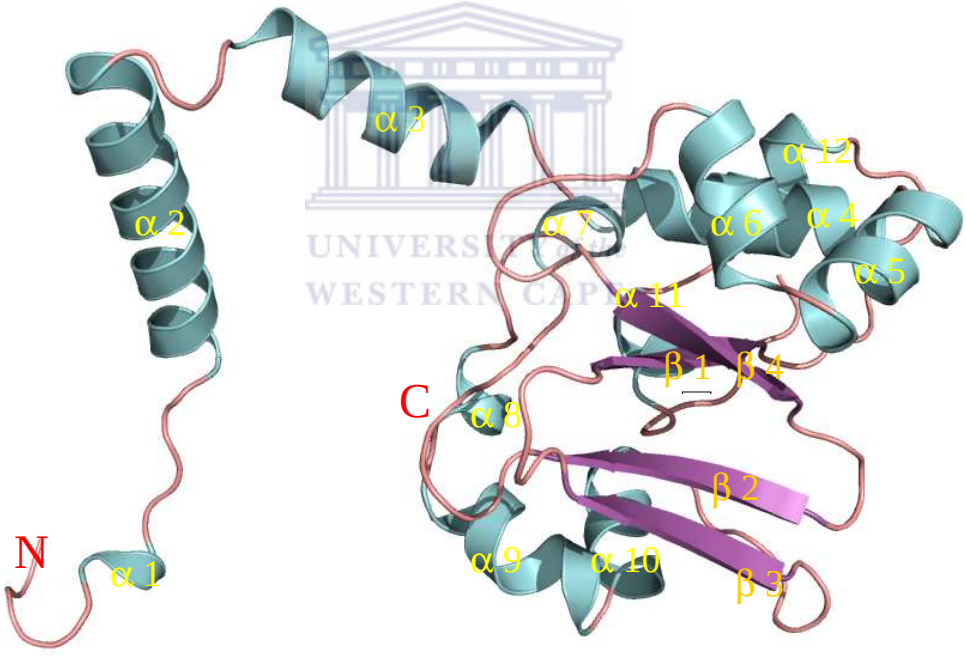

Figure 1.5: Cartoon representation of the α-subunit. Helixes are shown in cyan, sheets in purple and loops in violet.

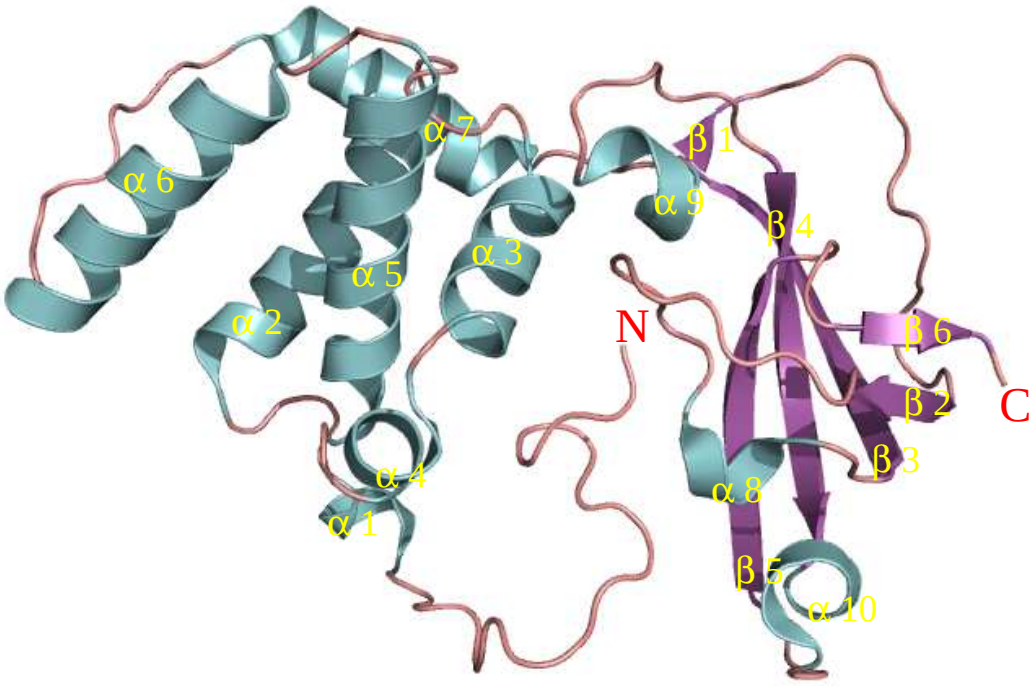

Figure 1.6: Cartoon representation of the β-subunit. Helixes are shown in cyan, sheets in purple and loops in violet.

1.4.5 Structural comparison of NHases

Most NHases are 2α2β heterotetramers with a few exceptions, the *Rhodococcus rhodochrous* J1 high molecular mass NHase (H-NHase) is a 10α10β in its native form (Kobayashi *et al*., 1991). The *Corynebacterium* sp. C5 NHase is a 2α homodimer (Yamamoto *et al*., 1992). Four NHase structures from different organisms are available in the Protein Data bank, a *G. pallidus* RAPc8 NHase (Cameron *et al*., 2005), *Bacillus smithii* SC-J05-1 (Hourai *et al*., 2003), a *Pseudonocardia thermophila* JCM 3095 (Miyanaga *et al*., 2001) and *Rhodococcus* sp. R312 (Huang *et al*., 1997). The *Rhodococcus* sp. R312 has the largest RMSD (Table 1.3**)** compared to the *G. pallidus* RAPc8 NHase but the overall fold is conserved (Fig 1.7). This is consistent with the fact that *Rhodococcus* sp. R312 is a mesophilic iron-type NHase, whereas other NHases are thermophilic cobalt types. Structural alignment shows an extra helix in the *G. pallidus* RAPc8 structure not present in the *Rhodococcus* sp. R312 structure (Fig 1.8).

The helix is involved in the interaction between the dimers in the heterotetramer, which may provide the increased thermostability in thermophilic NHases compared to the mesophilic Fe-type counterparts (Tsekoa, 2005).

Table 1.3: Details of structural alignment between *G. pallidus* RAPc8 NHase and other NHases.

Source of NHase	PDB accession no	No of cα atoms superimposed	r.m.s.d
Pseudonocardia thermophila JCM 3095	1 ire	373	1.051
Bacillus smithii SC-J05-1	1v29	389	0.329
Rhodococcus sp. R312	1ahj	303	0.959

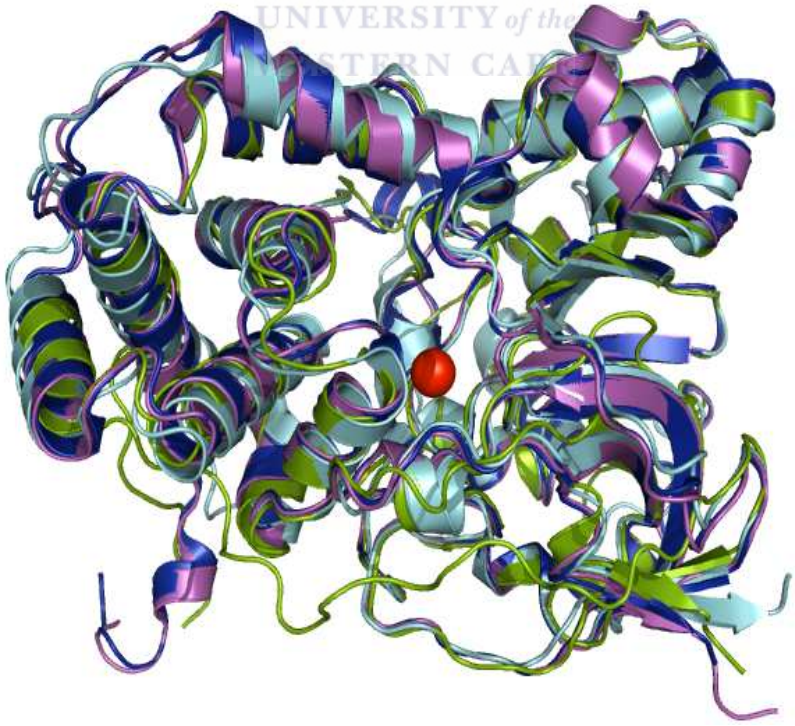

Figure 1.7: Structural alignment of NHases. *G. pallidus* RAPc8 NHase (2dpp) (blue), *Bacillus smithii* SC-J05-1 (1v29) (magenta), *Pseudonocardia Thermophila* JCM 3095 (1ire) (cyan), *Rhodococcus* sp. R312 (1ahj) (green).

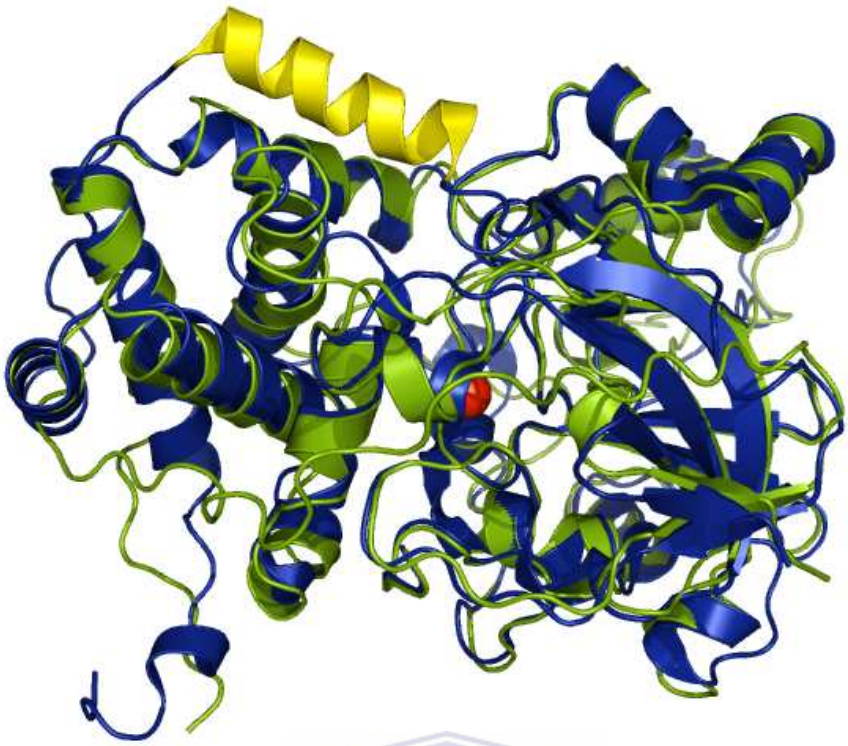

Figure 1.8: Structural alignment between the *G. pallidus* RAPc8 NHase (blue) (extra helix in yellow) and *Rhodococcus* sp. R312 (green).

1.4.6 Reaction mechanism of NHases

Nelson and colleagues proposed three mechanisms (Fig 1.9) for nitrile bioconversion to amides by NHase from the structure of the Fe-type NHase from *Rhodococcus* sp. R312 (Huang *et al.*, 1997). Subsequent proposed mechanisms are all generics of the first three mechanisms. The most widely accepted mechanism is the inner-sphere mechanism, which starts with the displacement of a metal ion coordinated hydroxide ligand by a nitrile substrate. The metal coordinated nitrile is hydrolysed, forming an imminolate intermediate, which is still coordinated to the metal ion. Tautomerism of the imminolate intermediate leads to the release of an amide product. Using the crystal structure of a co-type NHase from *Pseudonocardia thermophila* JCM 3095, in conjunction with kinetic, EPR, UV visible and theoretical studies, evidence was given in support of the inner-sphere mechanism (Fig 1.10) (Mitra and Holz, 2007).

Further evidence in support of the inner-sphere mechanism was given in a time resolved x-ray crystallography study using *Rhodococcus erythropolis* N771 NHase crystals soaked in *tert*-butylisonitrile (Hashimoto *et al.*, 2008). The study exploited the photoactivation of nitrosylated Fe-type *Rhodococcus erythropolis* N771 NHase (Endo and Odaka, 2000) and the slow reactivity of *tert*-butylisonitrile. The reaction of *tert*-butylisonitrile soaked NHase was induced by photo-induced denitrosylation of the NHase and stopped by flash cooling. At 120 minutes after photo-induced denitrosylation an electron density of *tert*-butylisonitrile coordinated to the iron ion centre was observed. After 440 minutes, a new electron density was observed near the isonitrile carbon and the sulfenate oxygen of αCys114, suggesting that the isonitrile binds directly to the metal ion and is then attacked by a nucleophile water molecule activated by cysteine-sulfenic acid 114 (αCys114-SOH).

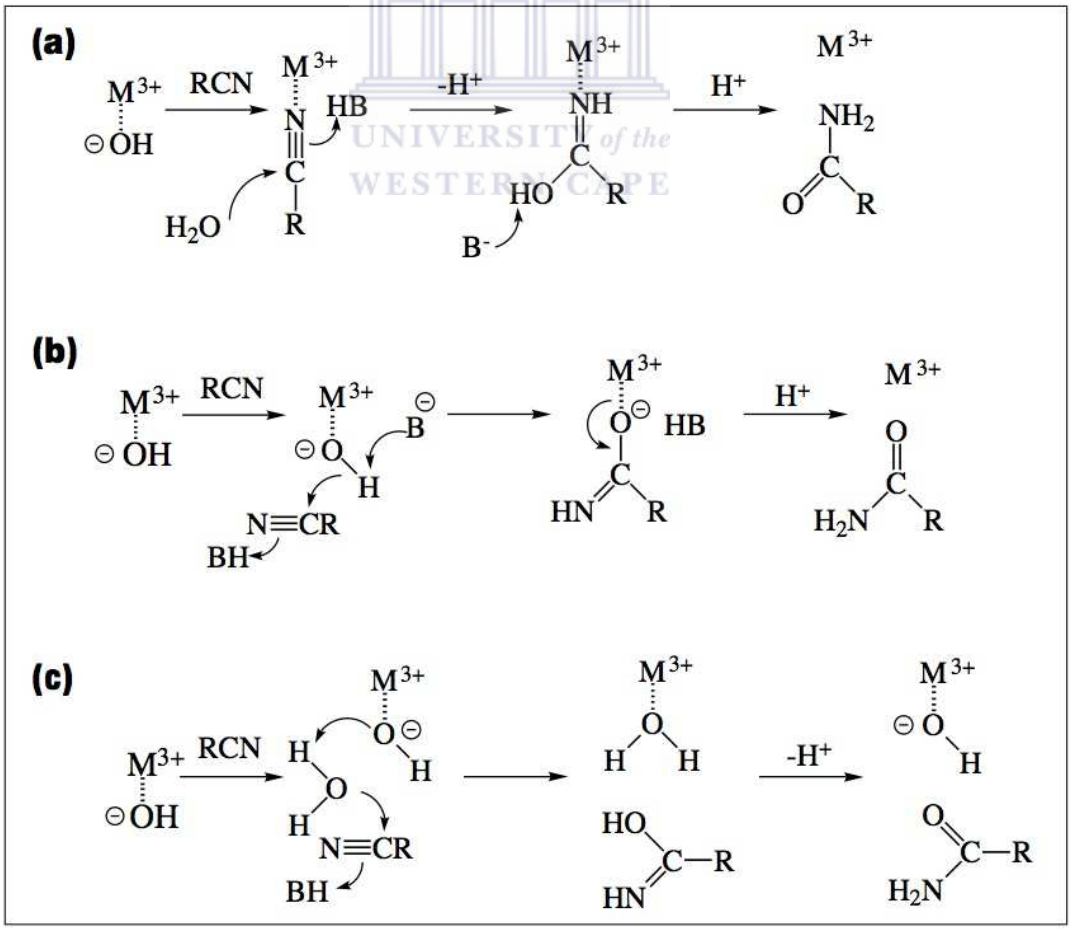

Figure 1.9: Proposed mechanisms for NHases. a) The inner-sphere mechanism. b) The outer-sphere mechanism. c) The second outer-sphere mechanism (Huang *et al*., 1997).

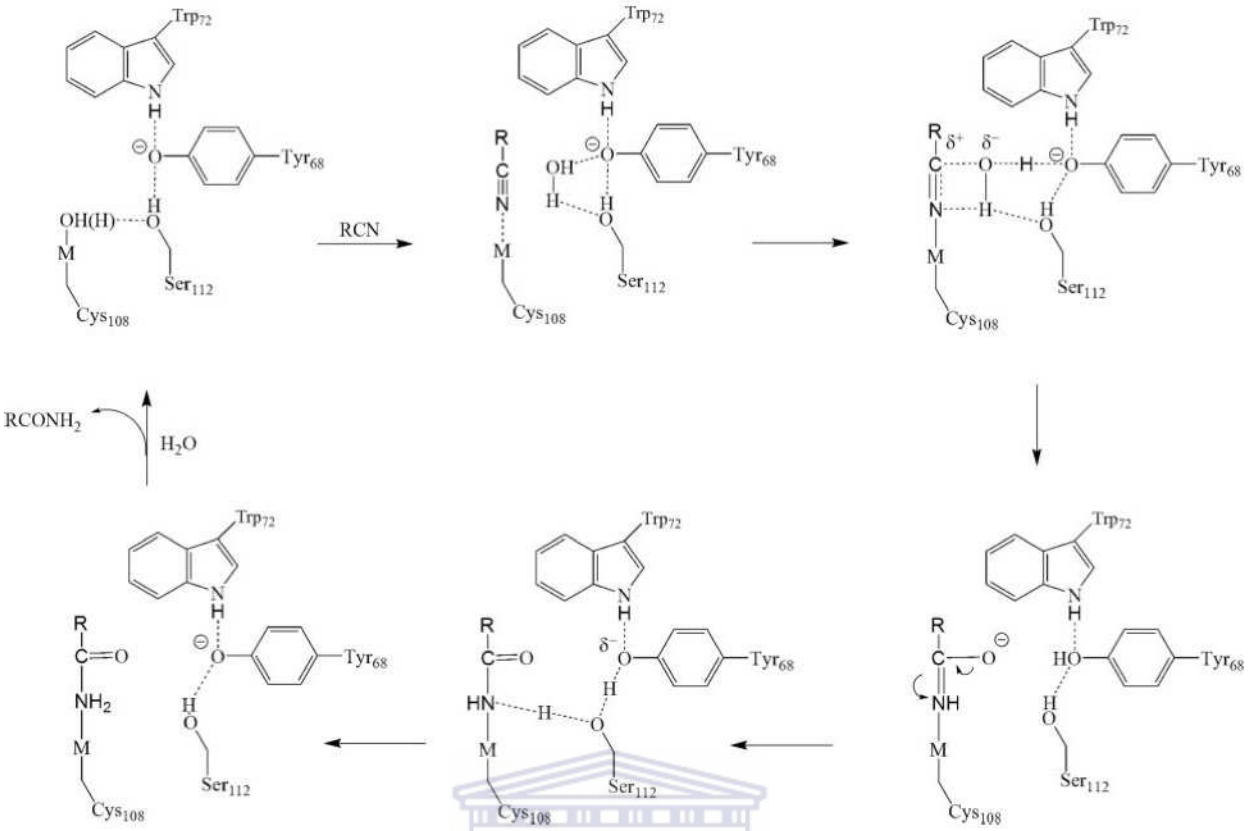

Figure 1.10: Proposed mechanism for nitrile bioconversion by NHases (Mitra and Holz, 2006).

The second mechanism (outer–sphere mechanism) starts with the nucleophilic attack of a nitrile substrate by a metal coordinated hydroxide ion forming an imminolate, which is oxygen bound to the metal ion. The imminolate tautomerises to an amide, which is then released from the active site. Mascharak (2002) proposed that the outer-sphere mechanism is the most likely for nitrile hydrolysis. This is based on the observation that the Co-type NHase from *Rhodococcus rhodochrous* and the Fe-type NHase from *Brevibacterium* R312 hydrolyze propionitrile at similar rates. When considering that the kinetics from the low spin Fe^{+3}(d5) and the Co^{+3}(d6) should be virtually distinct, it follows that the likely mechanism is that involving no ligand exchange. Song and colleagues provided evidence in support of the outer-sphere mechanism, while working on the crystal structure of a Fe-type NHase from *Rhodococcus erythropolis* AJ270 (Song *et al*., 2007). The structure revealed a double conformation of αGlu90 in the active site, implying that the residue is flexible (Fig 1.11a).

In one conformation the distance between αGlu90 and a water molecule is 2.15 Å, which suggests that αGlu90 interacts with the water molecule. The water molecule also interacts with the carbon of the cyano group indicated by the short distance (2.75 Å) between oxygen and carbon atoms. Based on these observations a mechanism for nitrile hydration by NHases was proposed (Fig 1.11b).

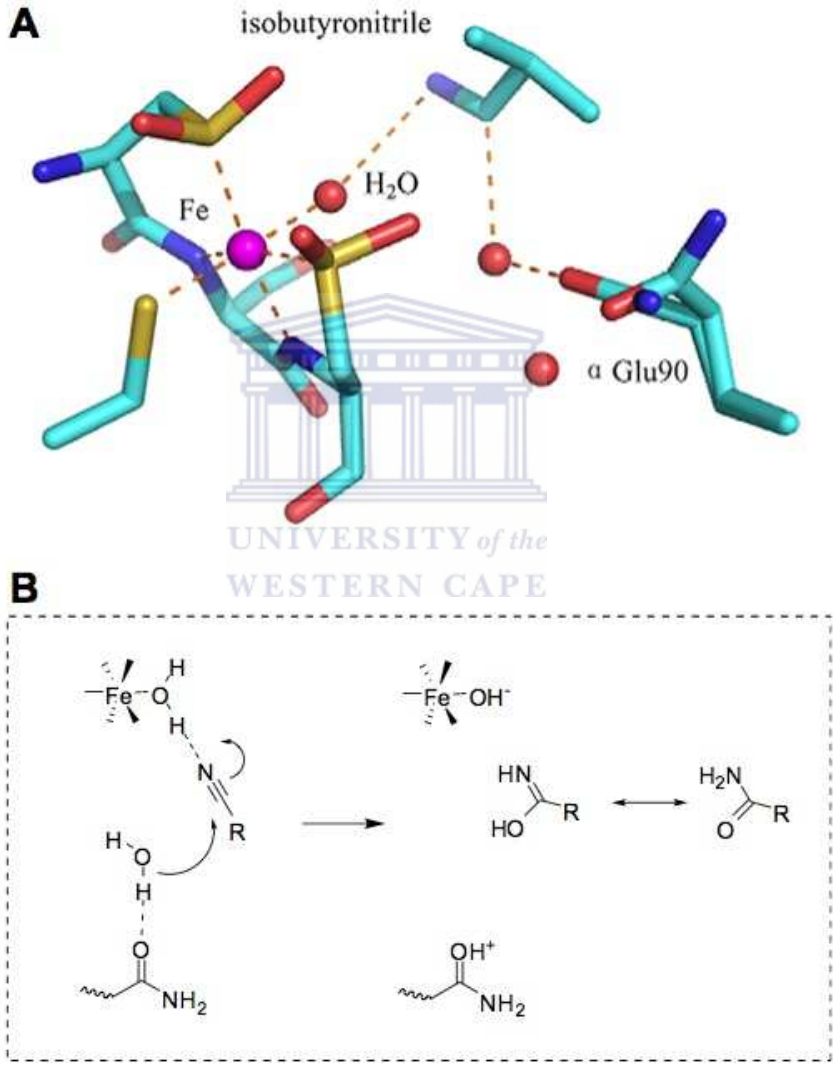

Figure 1.11: a) Alternative conformations of αGlu90 in the active site. b) Proposed mechanism for nitrile bioconversion by NHases (Song *et al*., 2007).

The third mechanism (second outer-sphere mechanism) starts with the deprotonation of a water molecule in the active site by the metal coordinated hydroxide ion forming a free hydroxide ion. The free hydroxide ion hydrolyses a nitrile substrate forming an imminolate intermediate, which tautomerises to the amide product. To the author's knowledge no structural evidence has been given in support of the second outer-sphere mechanism in the literature.

1.5 Application of NHases

1.5.1 Bioremediation

Nitriles are used extensively in the chemical and pharmaceutical industry for making a variety of compounds and polymers and as organic solvents. For example, acrylonitrile and adiponitrile are used for manufacturing polyacrylamide and nylon 66 polymers respectively in the chemical industry (Banerjee *et al.,* 2002). Nitriles are toxic compounds that have negative health effects and are known to be carcinogens (Ahmad and Farooqui, 1982). Effluents from these industries must be treated to detoxify and remove the nitriles prior to the release of the water into the environment. Microorganisms are known to use nitriles in energy metabolism (see section 1.2) and are therefore desirable for the treatment of nitrile effluents. Bacterial mixed cultures containing nitrile hydratases, amidases, and nitrilases have been reported to degrade 99% of detectable toxic nitrile compounds in continuous and batch culture systems (Wyatt and Knowles, 1995). Soil microorganisms have been shown to degrade 2,6-dichlorobenzonitrile (dichlobenil) to 2,6-dichlorobenzamide (BAM) the active component of herbicides Prefix G and Casoron G (Holtze *et al.,* 2006). An activated sludge consortium from a pharmaceutical treatment plant was shown to degrade acetonitrile, acrylonitrile and benzonitrile (Li *et al.*, 2007). Using recombinant DNA technology transgenic plants containing genes coding for nitrile metabolizing enzymes can possibly be used in the bioremediation of nitriles (Banerjee *et al*., 2002).

1.5.2 Biotransformations

Bioconversion of nitriles offers some benefits over chemical synthesis. Enzymes offer mild reaction conditions of temperature, pressure and pH. Extreme conditions of temperature and pH could have detrimental effects on important ester-linked functionalities (Cramp and Cowan, 1998). Enzymes also offer novel substrate, stereo- and regio-selectivity, which may not be attainable through chemical conversion (Benerjee *et al.,* 2002). The biggest application of NHases to synthetic chemistry is in acrylamide biosynthesis using a NHase from *Rhodococcus rhodochrous* J1 with a production of 30 000 tonnes per annum of acrylamide by the Nitto Chemical Company, Japan (Nagasawa and Yamada, 1995). Acrylamide is used as a precursor in the manufacture of acrylic fibres and plastics (Yamada and Kobayashi, 1996). The biotransformation of acrylonitrile to acrylamide is not only of industrial significance but of historical significance as well as this is the first successful example of a process for the biosynthesis of a commodity chemical (Yamada and Kobayashi, 1996). The NHase from *Rhodococcus rhodochrous* J1 is used for the synthesis of nicotinamide from 3-cyanopyridine (Mauger *et al*., 1988). Nicotinamide is known to assist in cartilage production and therefore is used in treatment of arthritis (Thomas *et al.,* 2002). Nicotinamide also forms part of anti-inflammatory agents such as Methylnicotinamide (Gebicki *et al*., 2003). Though industrial biotransformation is attractive, inhibition of certain enzymes (such as *G. pallidus* RAPc8 NHase) by their substrates (substrate inhibition), make such enzymes unsuitable for the industrial transformation of nitriles.

1.6 Substrate inhibition

The enzymatic conversion of substrate to product as described by the induced fit model starts with the binding of substrate molecule to the enzyme active site, forming an enzyme-substrate complex, which is followed by the conversion of substrate to product, described as follows for a one substrate reaction.

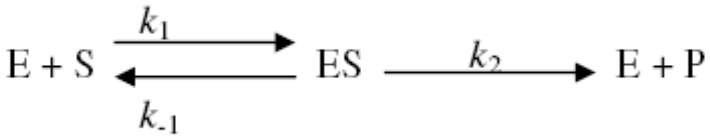

Under steady state kinetics the resulting derivation produces the classical Michaelis-Menten equation. Classical Michaelis-Menten kinetics are described by the equation $V=V_{max}*S/[S + K_M]$, V is the rate of the enzyme catalysed reaction, V_{max} is the theoretical maximum rate of the enzyme catalysed reaction, S is the substrate concentration and K_M is the substrate concentration at 1/2 V_{max} (Michaelis and Menten, 1913). The rate of an enzyme catalysed reaction increases with an increase in substrate concentration until a plateau is reached. In certain enzymes a phenomenon called substrate inhibition in enzymology and high-dose inhibition, autoinhibition, autoantagonism, autodesensitization, selfblokade, Arnudt-Schulz law or Arnudt-Schulz rule in pharmacology is observed (Kuhl, 1994). Substrate inhibition is a special case of uncompetitive inhibition, where binding of a second substrate molecule to the enzyme substrate-complex results in an ineffective enzyme substrate-substrate complex (Pastrana *et al*., 1998). Classical uncompetitive inhibition and substrate inhibition are pronounced at high substrate concentration when at any point in time an enzyme molecule has a substrate bound to the active site. Substrate inhibition is a rare physiological phenomenon, hence not much theoretical literature on the subject is available (Cornish-Bowden, 1986). The formation of the enzyme substrate-substrate complex during substrate inhibition is described as follows under steady state conditions.

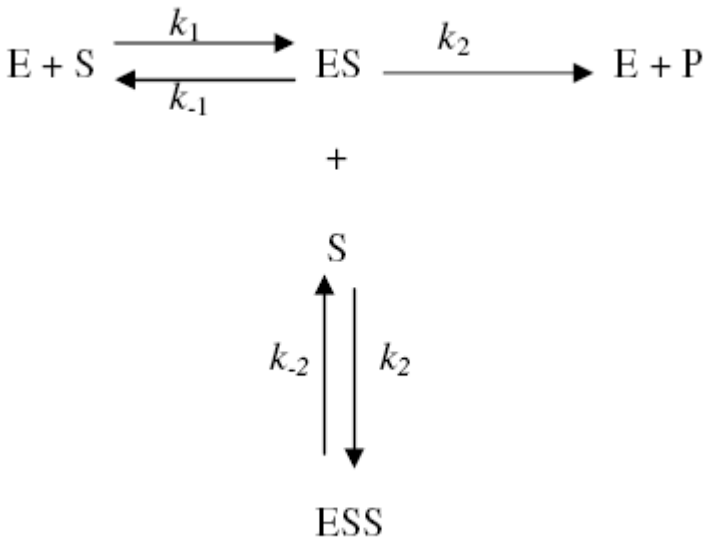

The Michaelis-Menten model transforms to the Briggs-Haldane (Substrate inhibition) model under substrate inhibition, which is described by the equation $V=V_{max}*S/[S + K_M + S^2/K_i]$ were K_i is the substrate inhibition constant (Cornish-Bowden, 1995). A number of models have been given to account for the molecular basis of substrate inhibition. In the Briggs-Haldane model, the enzyme groups required for catalysis must specifically interact with a substrate molecule for the enzymatic reaction to occur. Specific interactions of each of the enzyme groups with a substrate molecule occur frequently at low substrate concentrations. At high substrate concentrations when more than one substrate molecule occupies the active site, not all the enzyme groups interact with the substrate molecule leading to an ineffective enzyme-substrate complex. Another model, the recovery model incorporates a recovery phase for an effective enzyme-substrate complex to occur, where the substrate molecule must bind to the enzyme after the recovery phase (Kuhl, 1994). When the substrate molecule binds before the recovery phase has elapsed, the result is substrate inhibition. The chances of substrate binding during the recovery phase increases with substrate concentration, resulting in substrate inhibition being pronounce at high substrate concentrations. In enzymatic reactions such as hydration reactions (e.g. NHases) (see section 1.4.7), water is one of the reactants, high substrate concentrations can effectively reduce the water concentration particularly in the active site resulting in a decreased rate of the enzymatic reaction.

1.7 Aims

To investigate the molecular basis for substrate inhibition in *G. pallidus* RAPc8 NHases. Technical objectives include:

- Expression and purification of wild type and mutant NHases.
- Screening for changes in the substrate inhibition constant (K_i) of mutant NHases compared to the wild type enzyme.
- *In silico* modelling and analysis of wild type and mutant NHases.

Chapter 2: Materials and Methods

2.1 Chemicals and reagents

Chemicals of the highest available grade were supplied by Merck Chemicals and Laboratory Supplies™, Sigma-Aldrich Chemical™ Company and Kimix Chemical and Laboratory Supplies™.

Size markers (DNA and protein) and all DNA modifying enzymes (polymerases and restriction endonucleases) were purchased from Fermentas Life Sciences Ltd.

Oligonucleotide primers for polymerase chain reaction (PCR) were synthesized by Inqaba Biotech™.

2.2 Bacterial strains

Table 2.1: Bacterial strains used in this study.

Bacterial strain	Relevant Genotype	Supplier
E. coli BL21 (DE3)	hsdS gal ompT (cIts857 ind1 Sam7 nin5 lacUV5-T7 gene1)	Stratagene
E. coli BL21 pLysS	As above. [pLysS]	Stratagene

2.3 Expression plasmids

Table 2.2: Expression plasmids used in this study.

Plasmid	Description	Source
PET21a (+)	High-level expression vector containing an ampicillin resistance gene	Novagen
pNH14K (also known as pNH461)	A derivative of the pET21a (+) carrying the α and β subunit genes together with the P14K gene of the G. pallidus RAPc8 NHase	Cameron, 2002
pNH14K αW124G	NHase αW124G mutant of pNH14K	Cameron, 2002
pNH14K βW76G	NHase βW76G mutant of pNH14K	Tsekoa, 2005
pNH14K βF52GβF55L	NHase βF55LβF2G mutant of pNH14K	Kowlessur, 2007

2.4 Buffers and solution

Table 2.3: Buffers and solutions used in this study.

Buffer/Solution	Composition	pH
Agarose gel loading dye (6X)	0.25% (w/v) bromophenol blue 40% (w/v) sucrose	
Solution reagent A	0.59M phenol 1mM sodium nitroprusside	
Solution reagent B	0.11M sodium hypochlorite 2M sodium hydroxide	
1M Potassium phosphate buffer	717ml 1M K2HPO4 283ml 1M KHPO	7.2
SDS-PAGE electrode buffer (10X)	0.25M Tris-HCl 2M glycine 1% (w/v) SDS	8.3
SDS-PAGE Gel-loading Buffer (2X)	100mM Tris-HCl 4% (w/v) SDS	6.8
PAGE staining solution	0.2% (w/v) bromophenol blue 20% (v/v) glycerol 200mM dithiothreitol	
PAGE destaining solution	40% (v/v) methanol 10% (v/v) acetic acid	8.3
20X TAE buffer	2M Tris base 25mM EDTA (pH adjusted with glacial acetic acid)	

2.5 Protein expression

Wild type and mutant NHases were recombinantly expressed in *E. coli* BL21 pLysS or *E. coli* BL21 (DE3) (Stratagene). A 250ml LB culture containing 50μg/ml ampicillin and 30μg/ml chloramphenicol was grown at 37°C with shaking at 150rpm to an optical density of 0.4 at 600nm, followed by the addition of 0.1mM cobalt chloride, 15 – 30min before induction. Expression was induced with 0.4mM IPTG. Four hrs after induction cells were harvested by centrifugation and washed with 50mM potassium phosphate buffer, pH 7.2.

2.6 Protein purification

2.6.1 Cell free extracts preparation

Washed cell pellets were resuspended in 20ml of 50mM potassium phosphate buffer, pH 7.2. Cells were disrupted by one cycle of freezing at -80°C and thawing at 37°C followed by sonication (Bandelin Sonoplus HD2070 sonicator) in cycles of 30sec pulse, 30sec stop for 8min at 50% power. The lysate was centrifuged at 5000 x g for 20min and the supernatant collected.

2.6.2 Hydrophobic interaction chromatography (HIC)

Solid ammonium sulphate was added to 20% saturation (Appendix 1). Precipitated proteins were removed by centrifugation at 7000 x g for 30min at 4°C. The supernatant was loaded onto a HighLoad 16/10 Phenyl-Sepharose™ column (Amersham Biosciences) equilibrated with buffer containing (1M ammonium sulphate, 50mM potassium phosphate, pH 7.2). Bound proteins were eluted with a linear gradient of decreasing ammonium sulphate concentration generated with 50mM potassium phosphate buffer, pH 7.2 (5 column-volumes, 1M - 0M ammonium sulphate). NHase containing fractions were pooled and dialysed against 25mM potassium phosphate, pH 7.2.

2.7 Analytical Procedures

2.7.1 Spectrophotometry

Spectrophotometric analyses were carried out using a 300 *Bio* spectrophotometer™ operated *via* WinUV software (Varian Ltd).

2.7.2 Determination of protein concentration (Bradford assay)

The Bio-Rad™ Bradford Protein Assay reagent was used for determining protein concentration, using a 1ml assay volume (Bradford, 1976). Protein standards ranged from 0µg/ml to 10µg/ml bovine serum albumin (BSA) were constituted in 50mM potassium phosphate buffer. A standard curve is shown in Appendix 2.

2.7.3 Continuous enzyme kinetics

For the determination of $K_{i,}$ assays containing 50mM potassium phosphate, pH7.2 were conducted at 50°C in a 0.2cm quartz cuvette with a 0.7ml reaction volume. The following final concentrations of acrylonitrile dissolved in methanol 2.5, 5, 7.5, 10, 20, 30, 40, 50, 100, 150, 250, 350, 450, 550, 650, 750mM were used in the assays. The final concentration of methanol in the reaction volume was 5%. Reaction contents were incubated at 50°C to allow equilibration prior to the initiation of the reaction. The reaction was initiated by addition of 0.25µg of enzyme. The product of acrylonitrile hydration (acrylamide) was detected spectrophotometrically at 225nm.

2.7.4 Ammonia amidase coupled stop assay

For the determination of $K_{i,}$ assays containing 50mM potassium phosphate, pH7.2 were conducted at 50°C in 96 well microtitre plates using a 100µl final volume. The following final concentrations 2.5, 5, 7.5, 10, 20, 30, 40, 50, 100, 200, 300, 400, 500mM of 3-cyanopridine

dissolved in water were used in the assays. *G. pallidus* RAPc8 amidase was added in excess on ice. The reaction was initiated by the addition of 0.16µg of enzyme, allowed to run for 5min at 50°C and stopped by the addition of 100µl Solution A using a multichannel pipette. The contents were transferred to 1.5ml eppendorf tubes followed by the addition of 250µl of Solution A and then 350µl of Solution B. The constituents were then incubated for 5 min at 50°C and the absorbance measured spectrophotometrically at 600nm. The results were interpolated against a standard curve prepared using 0mM - 2mM ammonium chloride (Appendix 3).

2.7.5 Polyacrylamide gel electrophoresis (PAGE)

An adaptation of the Laemmli (1970) method was used to conduct SDS-PAGE on the Hoefer SE 250™ minigel electrophoresis unit. 0.75mm SDS-PAGE protein gels were prepared using a Hoefer SE 245™ dual gel caster. Tables 2.4 and 2.5 describe the components of the separating and stacking gel respectively. Gels were run at a voltage of 100V in 1X SDS-PAGE electrode buffer (Table 2.3). After electrophoresis gels were stained with coomassie blue, the stain was fixed by heating the gel in a microwave at 660-Watt for 15sec and allowed to stand for an hour, then destained using the PAGE destaining solution (Table 2.3).

Table 2.4: SDS PAGE (12%) separating gel components.

Components	Volume (ml)
ddH_2O	6.6
1.5M Tris-HCl, pH 8.8	5
20% (w/v) SDS	0.2
30% Acrylamide/0.8% Bis- acrylamide 0.8% (w/v)	8
10% (w/v) ammonium persulfate	0.2
TEMED	0.01

Table 2.5: SDS PAGE stacking gel components.

Components	Volume (ml)
ddH_2O	2.8
0.5M Tris-HCl, pH 6.8	1.25
20% (w/v) SDS	0.05
30% Acrylamide/0.8% Bis-acrylamide 0.8% (w/v)	0.85
10% (w/v) ammonium persulfate	0.05
TEMED	0.005

2.8 *In silico* protein modeling and analysis

All macromolecular structures were represented using PyMOL™ (Delano). Mutant NHase models were prepared using the mutagenesis tool in PyMOL.

Drawing of graphs and analysis of the enzyme kinetic data was conducted using Graphpad Prism 4 Software™ (Hearnes Corporation).

CASTp (Liang *et al.*, 1998) (http://sts-fw.bioengr.uic.edu/castp/calculation.php) was used to calculate cavity area and volumes. Cavities were visualised using Chime (Elsevier MDL). The default probe radius of 1.4 Å was used for all cavity calculations.

Molecular docking was conducted using Molegro Virtual Docker™ (Thomsen and Christensen, 2006) using substrate molecules made in PyMOL™ (Delano). The default options were used for molecule preparation in MVD. A single cavity was detected using the molecular surface option under the molecular surface caption. Under advanced settings a maximum cavity volume of 100000 was chosen and default values were chosen for all other captions. Default options were chosen to conduct the dockings under the docking wizard prompt.

Chapter 3: Expression and purification of *G. pallidus* RAPc8 NHases

3.1 Background

The *G. pallidus* RAPc8 bacterium formally (*Bacillus pallidus* RAPc8) was isolated from Australian lake sediments by repeated cycles of plating on selective (using aliphatic nitriles as the sole carbon source) and rich (nutrient agar) media (Pereira *et al.*, 1998). Wild type *G. pallidus* RAPc8 NHase is substrate specific for aliphatic, dinitrile and heteroaromatic substrates but not for homoaromatic substrates (Pereira *et al.*, 1998). Benzonitrile a homoaromatic nitrile was shown to be an uncompetitive inhibitor of the *G. pallidus* RAPc8 NHase (Tsekoa, 2005). The uncompetitive inhibition was attributed to possible interaction of π clouds in the aromatic substrate and the aromatic side chains of the residues lining the active site cavity. The solving of the crystal structure of *G. pallidus* RAPc8 NHase enabled the rational engineering of homoaromatic specificity into the enzyme (Tsekoa, 2005). Homoaromatic specificity was engineered into the enzyme through the construction of the βF52GFβ55L mutant (Kowlessur, 2007). The αW124G mutant has been shown to have reduced competitive inhibition compared to the wild type NHase (Cameron, 2002). Above all the wild type enzyme has been shown to be substrate inhibited at high substrate concentrations, which is undesirable for industrial bioconversion of nitriles to amides (Chiyanzu, 2008). This chapter describes the purification of the wild type, αW124G mutant and βF52GβF55L mutant for subsequent substrate inhibition analysis.

3.2 Expression of NHase genes

The *G. pallidus* RAPc8 NHase is constitutively expressed in the native organism. *G. pallidus* RAPc8 NHase was recombinantly expressed *in E. coli* BL21 under the *lac* promoter in the pET21a vector. The *E. coli* BL21 strain lacks the *lon* and the *OmpT* proteases resulting in high yields and greater stability of expressed proteins (Christensen *et al.*, 2004; Grodberg and Dunn, 1998). The supplementation of the growth media with 0.1mM $CoCl_2$ has been shown to increase the activity of expressed NHase (Tsekoa, 2005). Heat treatment of the apoenzyme in the presence of 5μM $CoCl_2$ for 45min at 50°C resulted in greater activity of expressed NHase (Tsekoa, 2005). Cloning the α and β subunits with a p14K auxiliary protein (see section 1.5.1) resulted in the highest activity of the expressed NHase (Table 3.1). Constructs containing the α and β subunits and the p14K auxiliary protein under a *lac* promoter were used for protein expression and the media supplemented with $CoCl_2$. Activity of the expressed NHases was confirmed by acrylonitrile hydration, measured spectrophotometrically at 225nm.

Table 3.1: Differential treatment of expressed NHase (Tsekoa, 2005).

Treatment	Activity (U/mg)
0.1mM $CoCl_2$ in growth medium	50
Heat-treatment of apoenzyme in presence of 5μM $CoCl_2$	450
Co-expression with P14K with 0.1mM $CoCl_2$ in growth medium	1600

3.3 Purification of NHases

The wild type and mutant NHases were purified using a modification of a previously described method (Tsekoa, 2005). A summary of the purification process is given in Table 3.2, Table 3.3 and Table 3.4 for the purification of the wild type, αW124G mutant, and the βF52GβF55L mutant respectively. Total protein extracts were subjected to ammonium sulphate precipitation at 20% w/v saturation. This step yielded 58% specific activity and 0.6-fold purification for the αW124G mutant. The yield and the purification fold for the αW124G is much lower compared to the wild type and the βF52GβF55L mutant. The decreased purification fold for the ammonium sulphate purification step compared to the total protein extracts indicates that the latter step resulted in contamination of the protein not purification.

All the enzymes had similar elution profiles on chromatograms and similar band patterns on SDS-PAGE, hence these are only shown for the αW124G mutant. Bound proteins on the HighLoad 16/10 Phenyl-Sepharose column were eluted by a decreasing gradient of ammonium sulphate generated using 50mM potassium sulphate buffer pH 7.2. The putative αW124G NHase mutant eluted approximately between 0.4 to 0.5M ammonium sulphate, corresponding to fractions 35 to 41 on the chromatogram (Fig 3.1). The resulting peaks were analysed on a 12% SDS-PAGE gel (Fig 3.2). A yield of 21% was obtained after HIC purification, which was lower compared to the wild type and βF52GβF55L mutant. A 23-fold purification was obtained for the αW124G mutant, which was higher than that obtained for the wild type and βF52GβF55L mutant. The specific activity for the αW124G mutant was comparable to that of the wild type and βF52GβF55L mutant. The purification process was followed on a 12% SDS PAGE gel and resulted in almost homogenous NHase protein (Fig 3.3, HIC insert).

Table 3.2: Purification table for the wild type NHase.

	Volume (ml)	Total Protein (mg)	Total Activity (Units)	Specific Activity (Units/mg)	Yield (%)	Purification (Fold)
Total protein extract	20	115	24895	216	100	1
Ammonium sulphate precipitation	19	109	38129	349	153	1.6
HIC	6	4.4	8627	1953	34	9

Table 3.3: Purification table for the αW124G mutant NHase.

	Volume (ml)	Total Protein (mg)	Total Activity (Units)	Specific Activity (Units/mg)	Yield (%)	Purification (Fold)
Total protein extract	20	78	6276	80	100	1
Ammonium sulphate precipitation	20	78	3655	47	58	0.6
HIC	5	0.695	1310	1885	21	23

Table 3.4: Purification table for the βF52GβF55L NHase mutant.

	Volume (ml)	Total Protein (mg)	Total Activity (Units)	Specific Activity (Units/mg)	Yield (%)	Purification (Fold)
Total protein extract	21	120.4	28550	255	100	1
Ammonium sulphate precipitation	20	112	42412	379	146	1.5
HIC	6	4.2	9454	2274	33	9

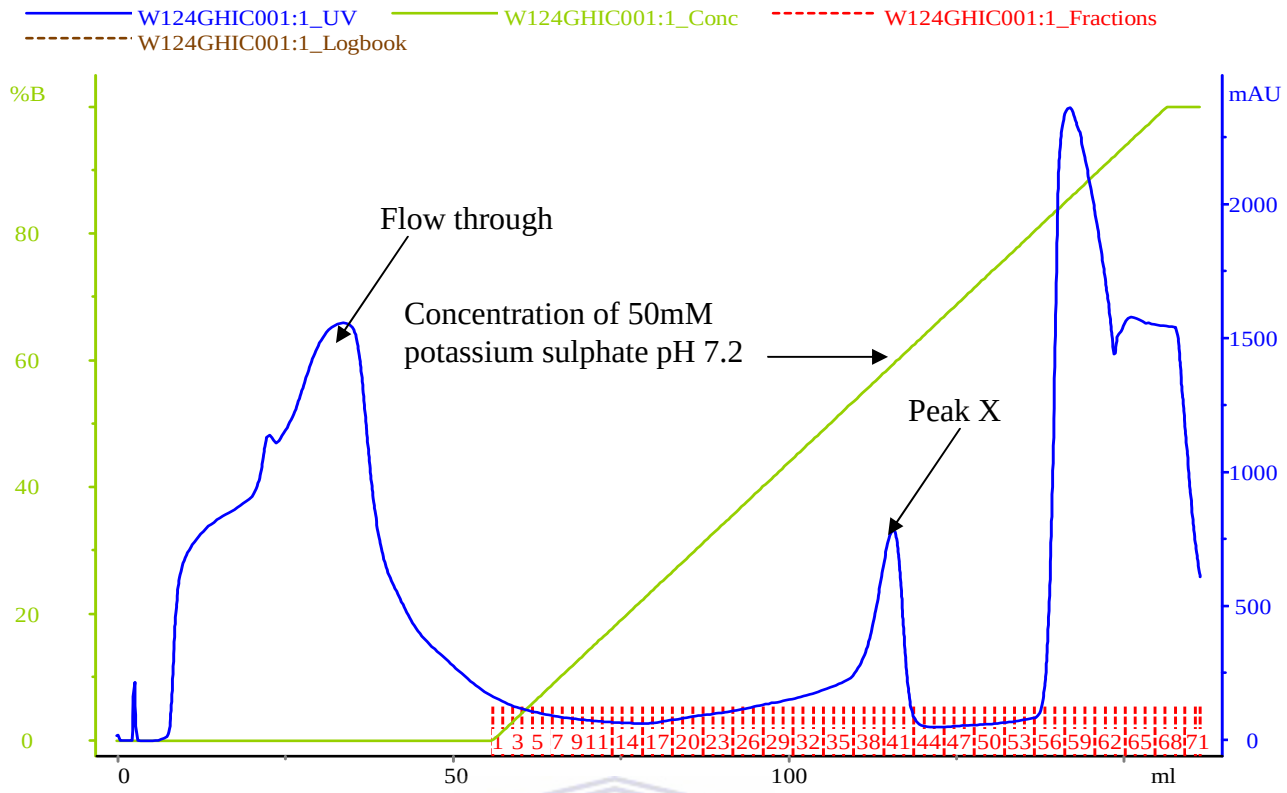

Figure 3.1: Chromatogram from Phenyl-Sepharose hydrophobic interaction chromatography. Peak X: corresponds to a putative αW124G mutant NHase.

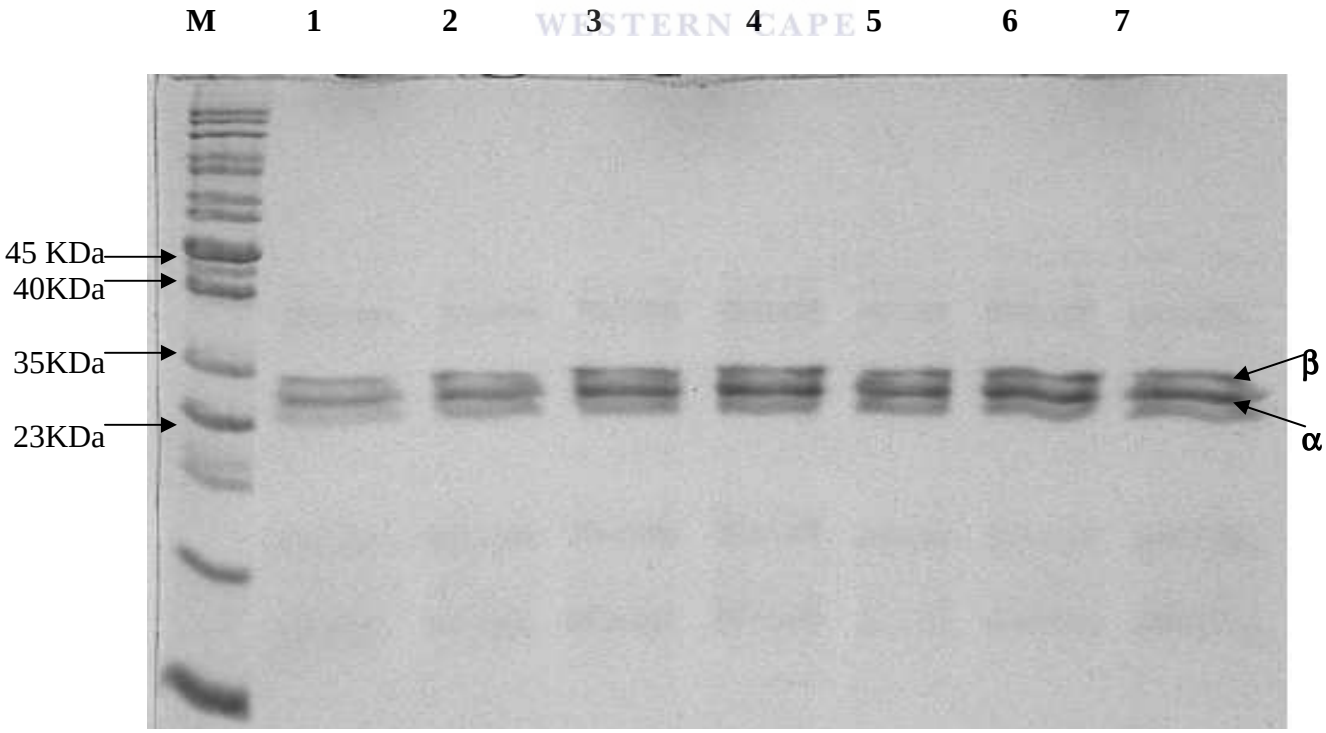

Figure 3.2: 12% SDS-PAGE analysis. Lane M: molecular marker, lanes 1-7: fractions 35-41 from HIC.

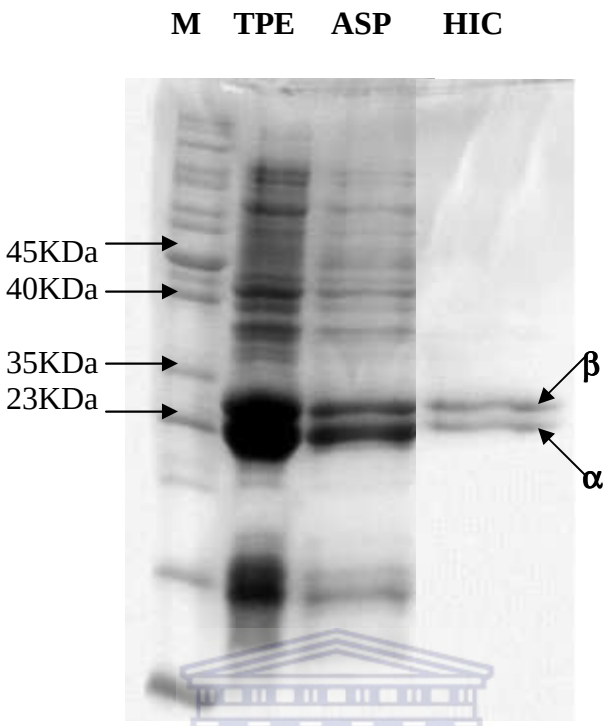

Figure 3.3: 12% SDS-PAGE analysis. M: Molecular marker, TPE: total protein extract, ASP: ammonium sulphate precipitation, (insert) HIC: hydrophobic interaction chromatography.

Chapter 4: Substrate inhibition enzyme kinetics and *in silico* protein modeling

4.1 Background

An ideal biocatalyst for industrial biotransformation needs to have a high turnover number (k_{cat}), a temperature optimum near the process operation temperature, high substrate selectivity, extended molecular stability and low substrate/product inhibition (Burton *et al.,* 2002). NHases are important biocatalysts for the conversion of nitriles to amides (see section 1.5.2). A turn over number between 1995-2340 s^{-1} (Kowlessur, 2007) and a temperature and pH optima of 50°C and 7.2 (Pereira *et al.,* 1998), respectively were determined for the *G. pallidus* RAPc8 NHase. The *G. pallidus* RAPc8 NHase has a broad substrate specificity range transforming a wide variety of nitriles, which include linear and branched aliphatics, heteroaromatics (3-cyanopyridine) and dinitriles, however not homoaromatic (benzonitrile) substrates (Pereira *et al.,* 1998). The lack of activity on benzonitrile was attributed to hydrophobic interactions between the substrate and the active site residues, resulting in the trapping of the substrate in a catalytically ineffective orientation (Tsekoa, 2005). 3-cyanopyridine has a lower electron density in the aromatic ring compared to benzonitrile, resulting in weaker hydrophobic interactions between the substrate and hydrophobic active site residues (Chiyanzu, 2008). This results in the substrate being able to assume a catalytically active orientation in the active site. Homoaromatic specificity was obtained with the engineering of the β52GβF55L double mutant (Kowlessur, 2007). Furthermore, the wild type shows substrate inhibition, a special case of uncompetitive inhibition (see section 1.6), which is undesirable for industrial biotransformation. This chapter describes the substrate inhibition kinetics and the *in silico* modelling and analysis of the wild type and mutant *G. pallidus* RAPc8 NHases.

4.2 Substrate inhibition kinetics

Substrate inhibition kinetics were conducted on the wild type and mutant *G. pallidus* RAPc8 NHases and the substrate inhibition constants (K_i) were determined in order to identify mutants exhibiting increased substrate tolerance compared to the wild type. For the substrate 3-cyanopyridine, which has a spectral absorbance at 235nm, the absorbance of the substrate is 10 at high substrate concentrations (data not shown). This means that 100% of the light is absorbed prior to product detection upon adding enzyme. The π electron clouds of the aromatic ring are the cause of the high absorbance in the substrate. The amidase coupled ammonium stop assay, which detects ammonia (at 600nm the byproduct of amide hydration by amidase) was used instead to conduct substrate inhibition assays for 3-cyanopyridine.

All the enzymes were strongly inhibited by 3-cyanopyridine at concentrations higher than 10mM. Visual inspection of the curves showed that only the Briggs-Haldane model fitted into the experimental data (Fig 4.1; Fig 4.2; Fig 4.3). Table 4.1 lists the best-fit values for the kinetic constants from Briggs-Haldane model for the hydration of 3-cyanopyridine by the wild type and mutant *G. pallidus* RAPc8 NHases. The βF52GFβ55L mutations resulted in a 2.3-fold reduction in K_M. This could arise from possible decreased hydrophobic interactions through the π electron clouds of the substrate with the side chains of the amino acids lining the active site cavity. As a result the substrate can easily assume a catalytically correct orientation. The αW124G mutation resulted in a 43.7-fold increase in K_M. The αW124 residue is conserved throughout all NHases indicating a structural or catalytic importance of the residue (Cameron, 2002). The βF52GFβ55L mutant had a 1.2-fold increase in K_i compared to the wild type, indicating a 1.2-fold decrease in the strength of substrate inhibition by 3-cyanopyridine. The αW124G mutant had a 50.3-fold decrease in K_i compared to the wild type, indicating a 50.3-fold increase in the strength of substrate inhibition in the mutant by 3-cyanopyridine compared to the wild type. Time constraints precluded the purification of the βW76G mutant.

However, crude extracts of the βW76G mutant (K_i = 1042mM) had a 46-fold decrease in substrate inhibition compared to the purified wild type enzyme.

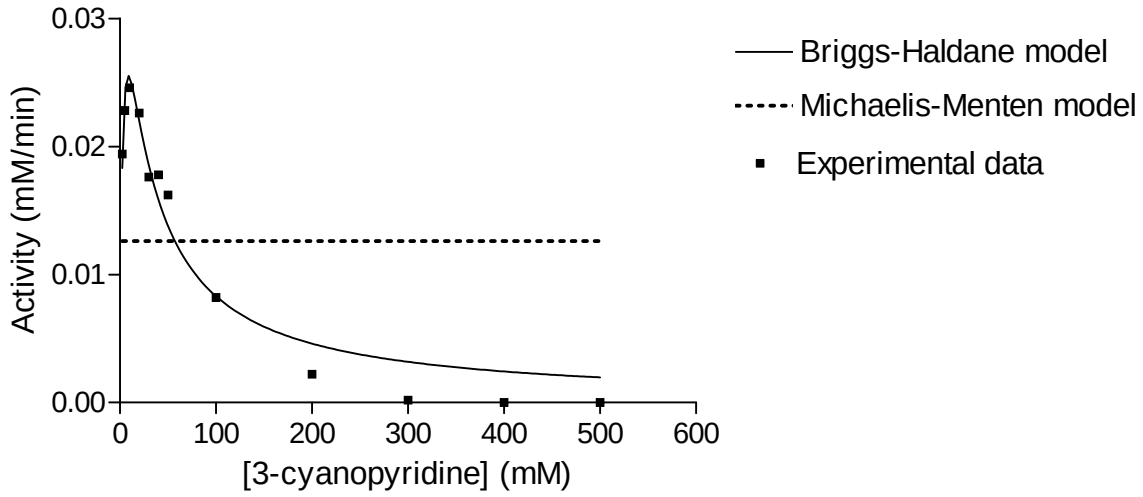

Figure 4.1: Michaelis-Menten and Briggs-Haldane curve for the wild type using 3-cyanopyridine as a substrate.

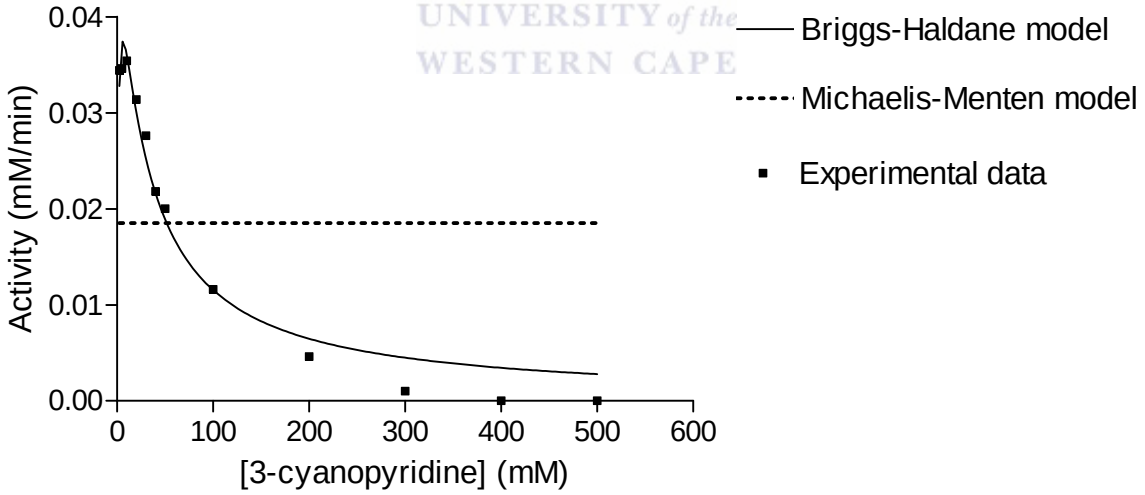

Figure 4.2: Michaelis-Menten and Briggs-Haldane curve for the βF52GβF55L mutant using 3-cyanopyridine as a substrate.

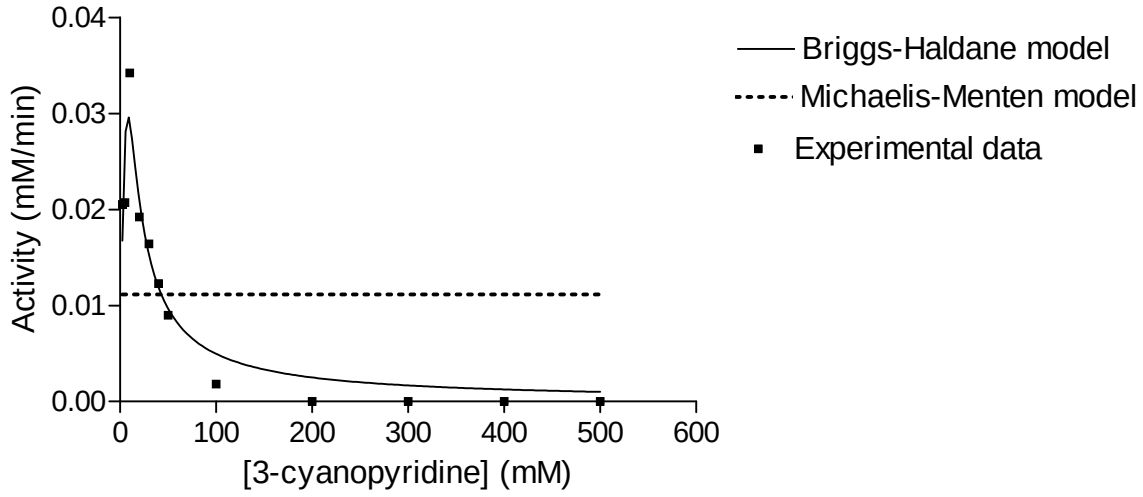

Figure 4.3: Michaelis-Menten and Briggs-Haldane curve for the αW124G mutant using 3-cyanopyridine as a substrate.

The standard error is used by Graph Pad Prism to calculate the 95% confidence limits of the best-fit values. The standard error is the expected standard deviation of a value if the experiment was conducted many times. The βF52GFβ55L mutant had the lowest standard error for K_M and K_i followed by the wild type and then the αW124G mutant. This means that the best-fit values for the αW124G mutant are the least accurate. The standard errors on graph pad are based on linear regression but applied to non-linear regression models, therefore may not give an accurate estimation of the standard error. The 95% confidence limit is a more accurate statistical parameter in describing the best-fit values. The 95% confidence limits for the mutants also suggested that the αW124G data was the least accurate, whilst the βF52GβF55L data was the most accurate.

The curve with the lowest absolute sum of squares (the distance of the Y-value of the points from the best-fit curve) is used by Graphpad Prism to calculate R^2 (the goodness of fit). R^2 is a misleading statistical indicator; it is an indication of how well the model fits the data and not an indication of the accuracy of the data. R^2 should therefore be viewed in conjunction with 95% confidence limits. The R^2 for the βF52GβF55L mutant was the highest of all the enzymes,

however overall the models fitted into the data very well. The standard deviation of residuals (Sy.x) is calculated from the absolute sum of squares and the degrees of freedom (the number of data points minus the number of parameters). It is an estimation of the accuracy of the dependent variables being measured; low values of this parameter indicate high accuracy of the dependent variable. Overall the statistics indicate good estimation of the best-fit values from all the models.

Table 4.1: Briggs-Haldane model kinetic constants for the wild type and mutant NHases for 3-cyanopyridine hydration.

		Mutant		
		Wild type	**βF52GβF55L**	**αW124G**
Best fit value	**K_M (mM)**	3.41	1.46	149.10
	K_i (mM)	22.67	26.76	0.45
Standard error	**K_M (mM)**	1.77	0.76	1732
	K_i (mM)	8.95	7.63	5.35
95% Confidence interval	**K_M (mM)**	0.0 to 7.40	0.0 to 3.17	0.0 to 4066
	K_i (mM)	2.42 to 42.92	9.49 to 44.02	0.0 to 12.54
Goodness of fit	**Degress of freedom**	9	9	9
	R^2	0.96	0.98	0.93
	Absolute Sum of Squares	2.55×10^{-2}	3.6×10^{-2}	6.7×10^{-2}
	Sy.x	2.05×10^{-3}	2.43×10^{-3}	3.33×10^{-3}

A 0.2cm path length quartz cuvette was used to conduct the direct enzyme on acrylonitrile. The spectrophotometric reading at high acrylonitrile concentrations exceeds two, which means that less than 1% of the light reaches the detector prior to product detection upon adding enzyme. A 0.2cm path length cuvette, theoretically allows for an 80% reduction in the absorbance of the substrate at any given concentration compared to the 1cm cuvette.

Low substrate inhibition by acrylonitrile was observed for the wild type (Fig 4.4), the βF52GβF55L mutant (Fig 4.5) and the αW124G mutant (Fig 4.6). The Michaelis-Menten model (Table 4.2) and the Briggs-Haldane model (Table 4.3) were fitted to the acrylonitrile experimental data. A 1.5-fold, 1.6-fold and a 3.8-fold increase in K_M for the wild type, βF52GβF55L and the αW124G mutant respectively was obtained when the Briggs-Haldane model was fitted to the data compared to the Michaelis-Menten model. This shows that the substrate binds with a lower affinity to the active site cleft when described by the Briggs-Haldane model. An approximately 100-fold increase in K_i was observed for the wild type and mutant NHases for acrylonitrile hydration compared to 3-cyanopyridine hydration. This is not surprising because aliphatic substrates have been shown to have the highest relative activity compared to aromatic substrates for *G. pallidus* RAPc8 NHase (Cameron, 2002). The wild type and βF52GβF55L mutant had the highest and approximately equal K_i values for acrylonitrile substrate inhibition (Table 4.3). The αW124G mutant had a 5.3-fold decrease in K_i compared to the wild type, hence it was most substrate inhibited by acrylonitrile. The αW124 residue is completely conserved throughout all NHases indicating a possible structural or catalytic significance (Cameron, 2002).

Narrow K_M 95% confidence limits were obtained for all the enzymes on both models, which means that the experimental data is well described by both models. Broad K_i 95% confidence limits were obtained for the wild type and βF52GβF55L mutant on the Briggs-Haldane model, indicating that the parameter (K_i) does not describe the experimental data very well. This shows

that the parameter is not essential for fitting a model into the data. The data is well defined by the Michaelis-Menten model, which indicates that the wild type and βF52GβF55L mutant have low substrate inhibition by acrylonitrile. This indicates the feasibility of using *G. pallidus* RAPc8 NHase for the industrial biotransformation of acrylonitrile to acrylamide. The αW124G mutant has the lowest 95% confidence limit for K_i and the lowest K_i meaning that it is substrate inhibited by acrylonitrile at high substrate concentrations. Good fits of the models into the data were achieved as indicated by the high R^2 on all the data sets for both models.

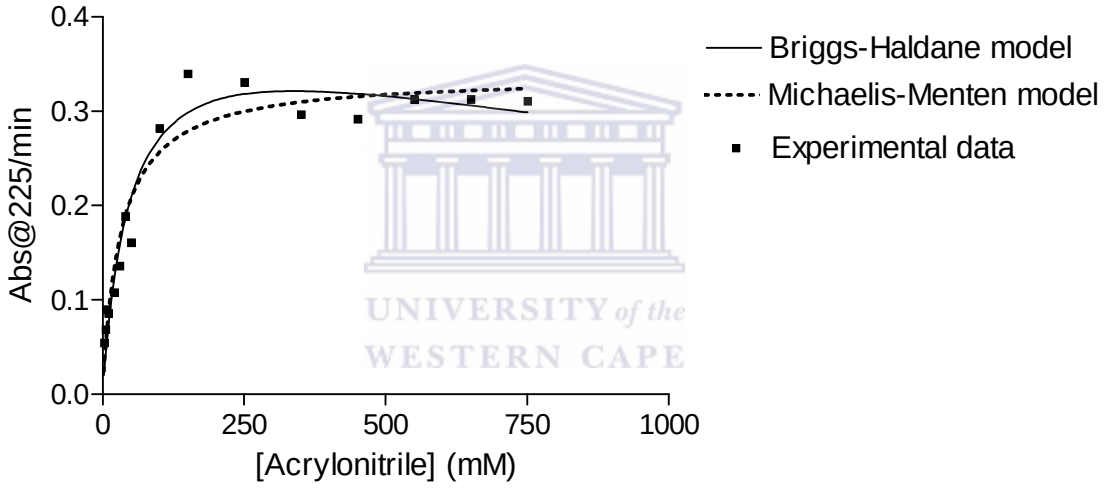

Figure 4.4: Michaelis-Menten and Briggs-Haldane curve for the wild type using acrylonitrile as a substrate.

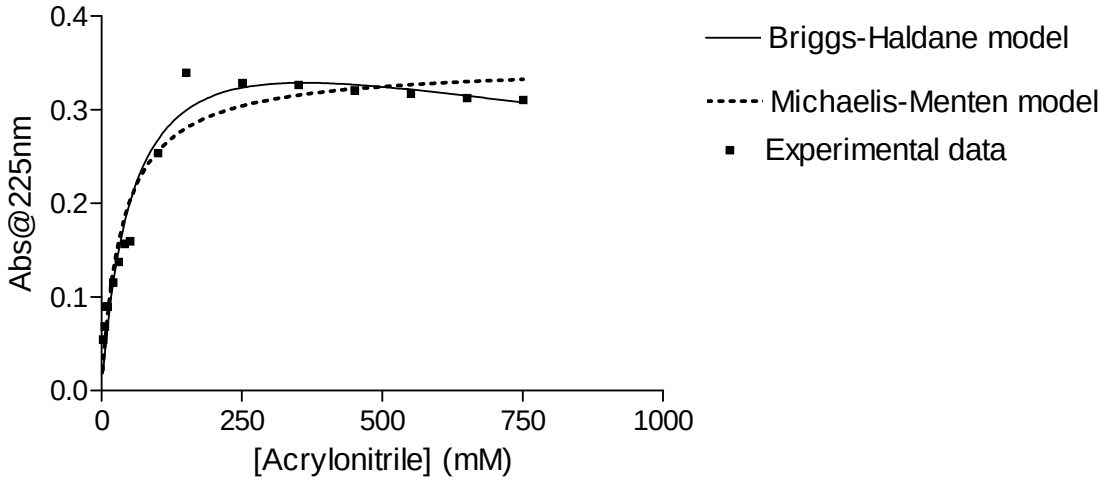

Figure 4.5: Michaelis-Menten and Briggs-Haldane curve for the βF52GβF55L mutant using acrylonitrile as a substrate.

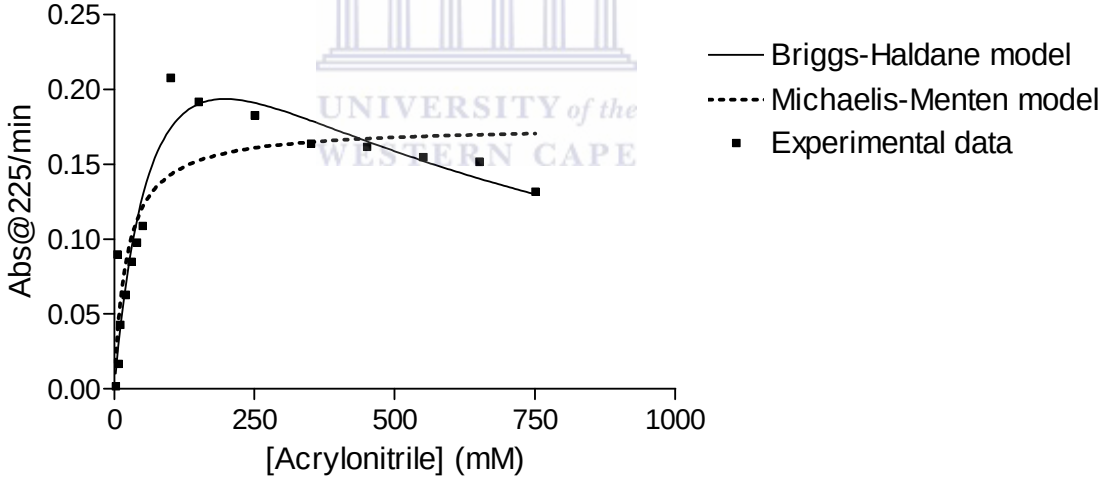

Figure 4.6: Michaelis-Menten and Briggs-Haldane curve for the αW124G mutant using acrylonitrile as a substrate.

Table 4.2: Michaelis-Menten model kinetic constants for the wild type and mutant NHases for acrylonitrile hydration.

		Mutant		
		Wild type	**βF52GβF55L**	**αW124G**
Best fit value	**K_M (mM)**	31.84	36.74	22.99
Standard error	**K_M (mM)**	6.06	6.58	8.79
95% Confidence interval	**K_M (mM)**	18.85 to 44.82	22.64 to 50.85	4.16 to 41.81
Goodness of fit	**Degress of freedom**	14	14	14
	R^2	0.93	0.94	0.77
	Absolute Sum of Squares	$1.19x10^{-2}$	$1.09x10^{-2}$	$1.37x10^{-3}$
	Sy.x	$2.92x10^{-2}$	$2.79x10^{-1}$	$3.12x10^{-2}$

Table 4.3: Briggs-Haldane model kinetic constants for the wild type and mutant NHases for acrylonitrile hydration.

		Mutant		
		Wild type	**βF52GβF55L**	**αW124G**
Best fit value	**K_M (mM)**	48.59	57.75	88.12
	K_i (mM)	2338	2243	441
Standard error	**K_M (mM)**	14.09	16.16	46.48
	K_i (mM)	1635	1503	270
95% Confidence interval	**K_M (mM)**	18.16 to 79.02	22.86 to 92.65	0.0 to 188.50
	K_i (mM)	0.0 to 5869	0.0 to 5489	0.0 to 1024
Goodness of fit	**Degress of freedom**	13	13	13
	R^2	0.94	0.95	0.88
	Absolute Sum of Squares	$9.88x10^{-3}$	$8.84x10^{-3}$	$7.38x10^{-3}$
	Sy.x	$2.76x10^{-2}$	$2.61x10^{-2}$	$2.38x10^{-2}$

4.3 *In silico* protein modeling

4.3.1 Cavity analysis

Tsekoa (2005) suggested that the increase in cavity dimensions was probably the single contributing factor for the reduction in the observed uncompetitive inhibition of the βW76G mutant by benzonitrile compared to the wild type. Time constraints precluded the purification of the βW76G mutant. However, crude extracts of the βW76G mutant (K_i = 1042mM) had a 46-fold decrease in substrate inhibition compared to the purified wild type enzyme. The decrease in substrate inhibition of the βW76G and βF52GβF55L mutants by 3-cyanopyridine, suggested that the βF52GβF55LβW76G triple mutant could possibly have a greater synergistic reduction in substrate inhibition by 3-cyanopyridine. Mutant *G. pallidus* RAPc8 NHase models were created using the mutagenesis tool in PyMOL on residues lining the substrate channel (Table 4.4). The tool has been shown to create mutant NHase models with similar channel dimensions as those of experimentally determined crystal structures (Tsekoa, 2005). CASTp was used to determine the dimensions of the cavity transversing the active site of the wild type and mutant NHase models (Table 4.5). A 15.8%, 16.3%, 20.2% and 13.5% increase in the area was observed for βF52GβF55L, βW76G, βF52GβF55LβW76G and αW124G respectively. In terms of volume a 19.7%, 16.8%, 27.5% and 16.5% increase was obtained respectively. Though an increase in cavity dimensions was observed for all the enzymes, this did not result in a decrease in substrate inhibition for all mutants. The αW124G mutation resulted in an increase in substrate inhibition by 3-cyanopyridine. Clearly there is no direct correlation between the cavity size and the strength of substrate inhibition.

Table 4.4: Amino acid residues lining the substrate channel of the wild type and mutant RAPc8 NHases.

Pocket	α-subunit	β-subunit
70	Leu96, Gln97, Glu99, Leu118 Ser120, Tyr122, Trp124, Leu129 Lys135, Glu136, Pro137, Arg140 Ser169, Ser170, Ser171, Glu172 Arg174	His5, Phe36, Gly48, Met49 Lys50, Ala51, Phe52, Asp53 Glu54, Phe55, Arg56, Ile59 Glu60, Tyr67, Leu68, Ser71 Tyr72, Tyr73, His75, Trp76 Thr87, Leu130, Pro132, Arg134 His158, Arg160, His179, Val180 Pro182, Ala185, Arg188, Gly190 Glu191, Trp220

Mutated residues are coloured in red.

Table 4.5: Cavity dimensions and substrate inhibition constants for the wild type and mutant NHases.

Mutant	Area (Å^2)	Volume (Å^3)	K_i (3-cyanopyridine)
Wild type	1179.5	1303.3	22.67
βF52GβF55L	1400.4	1622.2	26.76
βW76G	1409.7	1567.1	1042
βF52GβF55LβW76G	1477.7	1796.9	Un
αW124G	1364.3	1560.1	0.45

Un denotes undetermined.

4.3.2 Molecular docking

To test if the βF52GβF55LβW76G mutation could confer increased substrate tolerance to 3-cyanopyridine compared to the wild type; docking of acrylonitrile and 3-cyanopyridine to the wild type and mutant NHase models was conducted using Molegro Virtual Docker. The protein and ligands were prepared using the default settings and the cavity was detected using a 1.2Å probe radius (Fig 4.7). The cavity transverses the active site with the *claw-setting motif* located in the centre.

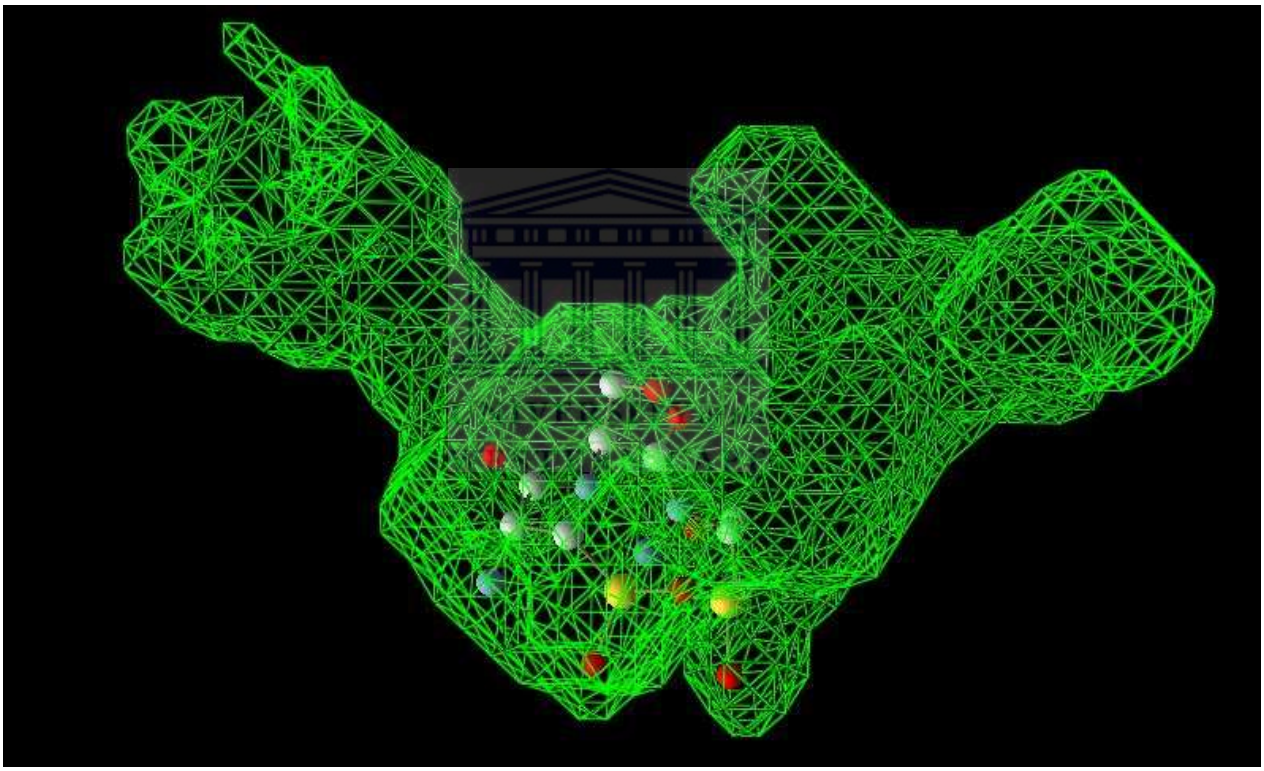

Figure 4.7: Cavity detected in *G. pallidus* RAPc8 NHase, claw setting motif in spheres (figure generated using Molegro Virtual Viewer).

The inner-sphere mechanism (see section 1.4.6), where nitriles bind directly to the metal ion centre was assumed to be the correct mode of catalysis. Therefore, ligands that dock with the nitrile nitrogen orientated towards the cobalt metal ion were considered to be in a catalytically active orientation.

The ligands which docked with the highest energy, in a catalytically active orientation were chosen for analysis for each NHase model. Table 4.6 gives the rerank scores (energies) of docked acrylonitrile ligands and the distance of the nitrile nitrogen to the cobalt metal ion. Fig 4.8 displays the orientations of the nitrile nitrogens to cobalt metal ion centre for the docking of acrylonitrile. Acrylonitrile docked into the wild type with the highest (best) score and the shortest nitrile nitrogen to cobalt metal ion distance, followed by the βF52GβF55L mutant, both in the catalytically active orientation. Acrylonitrile docked into the βW76G mutant model with the lowest score of all models, in a catalytically active orientation and with a shorter nitrile nitrogen to cobalt metal ion distance compared to the βF52GβF55LβW76G and the αW124G mutant models. This is consistent with enzyme kinetic data, with the wild type, βF52GβF55L and βW76G mutants having good activities on acrylonitrile (Tsekoa, 2005; Kowlessur, 2007). A similar study using the crystal structure of the NHase from *Pseudonocardia thermophila* JCM 3095 showed that aliphatic nitriles docked with a higher propensity towards the active site metal ion compared to aromatic nitriles (Peplowski *et al*., 2007). The βF52GβF55LβW76G and αW124G mutant models had lower docking scores for acrylonitrile compared to the wild type and the βF52GβF55L mutant model, and the longest nitrile nitrogen to cobalt metal ion distances in a catalytically inactive orientation. This is consistent with the αW124G mutant displaying higher substrate inhibition by acrylonitrile compared to the wild type and βF52GβF55L mutant.

Table 4.6: Docking results of acrylonitrile into wild type and mutant NHase.

Mutant	Pose*	Rerank score	Distance of N to Co
Wild type	[02]Non_2	-28.69	4.52
βF52GβF55L	[04]Non_2	-29.36	6.57
βW76G	[02]Non_2	-34.70	7.86
βF52GβF55LβW76G	[01]Non_2	-32.30	10.11
αW124G	[02]Non_2	-30.38	10.81

***Pose is the conformation of docked ligands and the naming was arbitrarily given by MVD.**

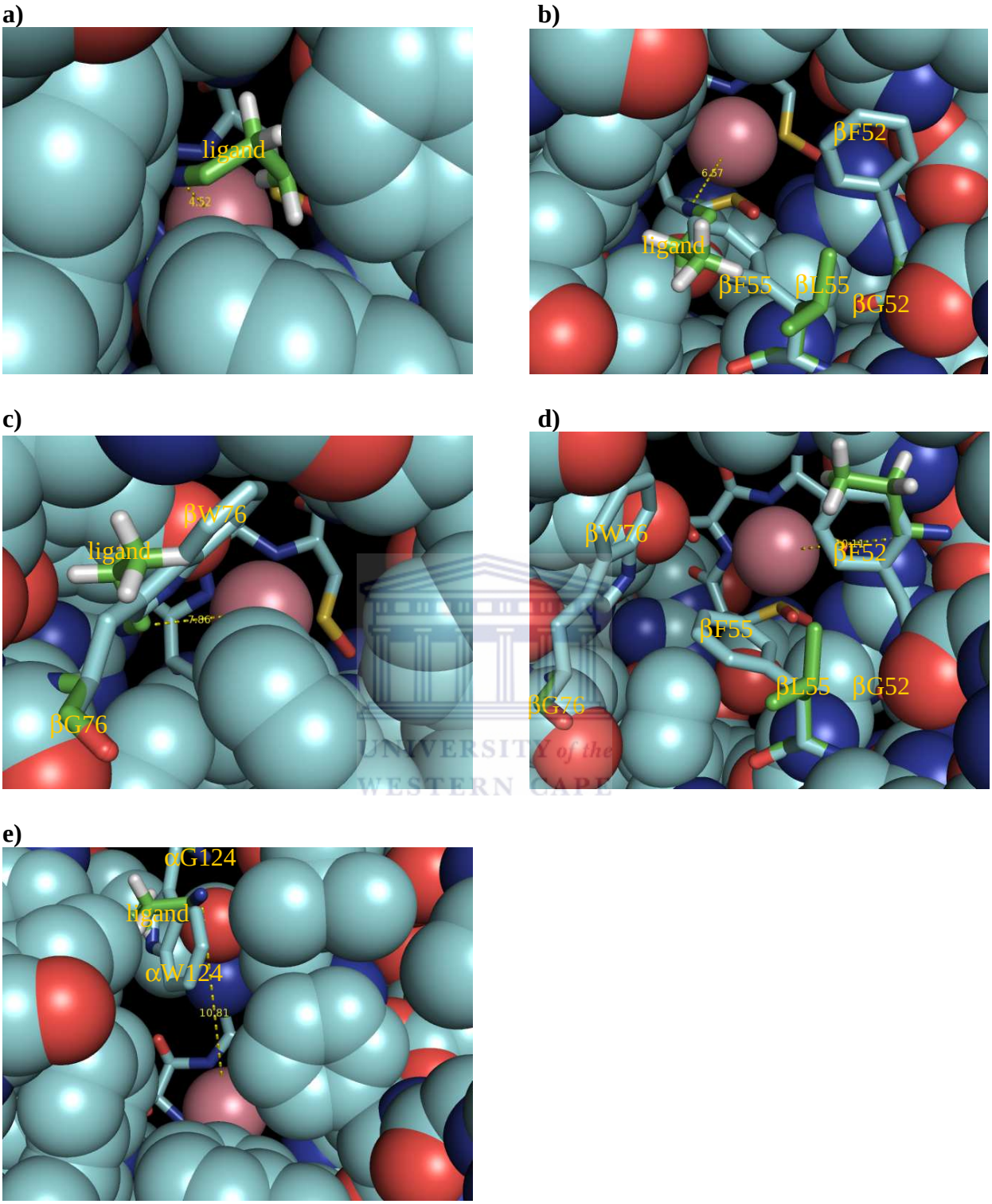

Figure 4.8: Orientations of docked acrylonitrile to wild type and mutant *G. pallidus* RAPc8 NHases. a) Wild type b) βF52GβF55L c) βW76G d) βF52GβF55LβW76G e) αW124G. Original residues are shown as cyan sticks, mutated residues and docked ligands are shown as green sticks.

The docking of 3-cyanopyridine to the wild type and mutant NHase models was conducted in order to find the mutant with the highest score and shortest nitrile nitrogen to cobalt metal ion distance in a catalytically active orientation for 3-cyanopyridine (Table 4.7). The assumption is that the mutant would have high activity on 3-cyanopyridine and reduced substrate (3-cyanopyridine) inhibition at elevated substrate concentrations compared to the wild type, just as the wild type has high activity and no substrate inhibition on acrylonitrile. Fig 4.9 displays the orientation of the nitrile nitrogen to the cobalt metal ion centre. For 3-cyanopyridine the wild type had the lowest score and nitrile nitrogen to cobalt metal ion distance, similar to that of the βW76G mutant model, however in a catalytically inactive orientation. 3-cyanopyridine docked to the βF52GβF55L mutant model with the highest score but had the longest nitrile nitrogen to cobalt metal ion distance in a catalytically inactive orientation. A dock into the αW124G mutant model with the third highest score in a catalytically active orientation was obtained. The best dock was obtained with the βF52GβF55LβW76G mutant model, which had the second highest score with a nitrile nitrogen to cobalt metal ion distance comparable to that of the wild type in a catalytically active orientation. These results indicate that the βF52GβF55LβW76G mutant could be suitable for the bioconversion of 3-cyanopyridine with little or no substrate inhibition just as the wild type is suitable for the conversion of acrylonitrile with no substrate inhibition.

Table 4.7: Docking results of 3-cyanopyridine into wild type and mutant NHases.

Mutant	Pose*	Rerank score	Distance of N to Co
Wild type	[02]NHH_2	-57.50	7.42
βF52GβF55L	[04]NHH_2	-47.57	10.12
βW76G	[00]NHH_2	-57.69	7.97
βF52GβF55LβW76G	[02]NHH_2	-51.11	7.99
αW124G	[02]NHH_2	-53.30	7.93

***Pose is the conformation of docked ligands and the naming was arbitrarily given by MVD.**

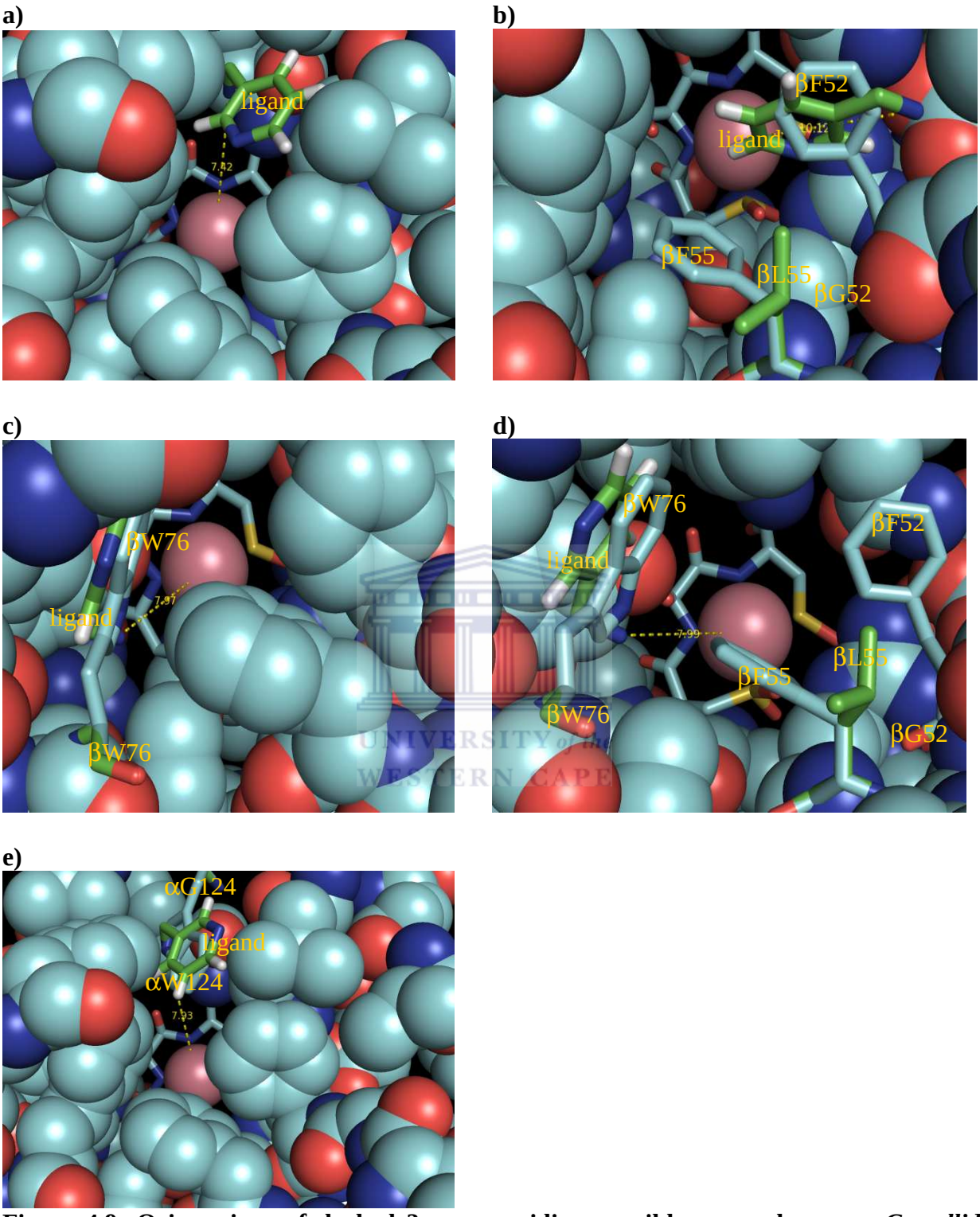

Figure 4.9: Orientations of docked 3-cyanopyridine to wild type and mutant *G. pallidus* RAPc8 NHases. a) Wild type b) βF52GβF55L c) βW76G d) βF52GβF55LβW76G e) αW124G. Original residues are shown as cyan sticks, mutated residues and docked ligands are shown as green sticks.

Chapter 5: General discussions

The aim of this work was to screen for *G. pallidus* RAPc8 NHase mutants with reduced substrate inhibition compared to the wild type enzyme. The substrate inhibition constant (K_i) was determined for the wild type and a range of mutant NHases using 3-cyanopyridine and acrylonitrile as substrates.

The enzymes displayed low substrate inhibition by acrylonitrile. The βF52GβF55L mutant, with a substrate inhibition constant K_i = 2243mM showed similar substrate inhibition kinetics to the wild type with a substrate inhibition constant K_i = 2338mM. The αW124G mutant displayed a 5.3-fold increase in substrate inhibition by acrylonitrile with a substrate inhibition constant, K_i = 441mM. All the enzymes showed high substrate inhibition by 3-cyanopyridine. The βF52GβF55L (K_i = 26.76mM) mutant had a 1.2-fold decrease in substrate inhibition by benzonitrile compared to the wild type (K_i = 22.67mM), while the αW124G (K_i = 0.45mM) mutant had a 50-fold increase in substrate inhibition. The results correlate with a previous report on the substrate inhibition of *G. pallidus* RAPc8 NHase by 3-cyanopyridine (Chiyanzu, 2008). The previous work consisted of the determination of the substrate inhibition constant for free and immobilised homogenous wild type *G. pallidus* RAPc8 NHase. Enzyme immobilisation resulted in a 52% decrease in substrate inhibition.

Previous work showed that the βW76G mutant has a more than 2-fold decrease in uncompetitive inhibition by benzonitrile compared to the wild type (Tsekoa, 2005). Preliminary experiments using crude extracts of the βW76G mutant showed a 46-fold reduction in substrate inhibition compared to the partially purified wild type enzyme. Cavity analysis of the wild type and mutant NHase models, showed an increase in the cavity dimensions of the mutants compared to the wild type. However, no direct correlation was observed between cavity size and substrate inhibition.

As an increase in cavity size in the αW124G mutant did not result in a decrease in substrate inhibition but an increase.

The possible synergistic effect of combining the βF52GβF55L mutant with the βW76G mutant to reduce the substrate inhibition was considered. The βW76GβF52GβF55L mutant model was constructed *in silico*, the cavity analysed and the substrates acrylonitrile and 3-cyanopyridine were docked into the βW76GβF52GβF55L mutant model and the wild type model. The results were analysed to observe changes in binding affinity of acrylonitrile and 3-cyanopyridine to the βW76GβF52GβF55L mutant model compared to the wild type model. Acrylonitrile docked into the wild type model with the highest score and the shortest nitrile nitrogen to cobalt metal ion distance in a catalytically active orientation. This is consistent with the enzyme kinetic data showing that the wild type is substrate specific for acrylonitrile, an aliphatic nitrile. 3-Cyanopyridine docked with the second highest score into the βF52GβF55LβW76G mutant model, with a nitrile nitrogen to cobalt metal ion distance comparable to that of the wild type in a catalytically active orientation. This indicates that the combined mutations could possibly reduce substrate inhibition in *G. pallidus* RAPc8 NHase by 3-cyanopyrine and other aromatic nitriles such as benzonitrile.

The mutant must be constructed and substrate (3-cyanopyridine) inhibition kinetics conducted in order to validate the *in silico* results. To possibly further reduce the substrate inhibition, the mutant must be immobilised, which has been shown previously to reduce substrate inhibition by 3-cyanopyridine by 52% in the wild type *G. pallidus* RAPc8 NHase (Chiyanzu, 2008). This study and previous others indicate that *G. pallidus* RAPc8 NHases could possibly be applicable in the industrial bioconversion of nitriles to amides.

References

Ahmed, A. E. and Farooqui, M. Y. H. (1982) Comparative toxicities of aliphatic nitriles. Toxicology Letters. 12, 157-163

Arakawa, T., Kawano, Y., Kataoka, S., Katayama, Y., Kamiya, N., Yohda, M. and Odaka, M. (2007) Structure of Thiocyanate Hydrolase: A New Nitrile Hydratase Family Protein with a Novel Five-coordinate Cobalt (III) Center. Journal of Molecular Biology. 366, 1497–1509

Asano, Y. and Kato, Y. (1998) Z-phenylacetaldoxime degradation by a novel aldoxime dehydratase from Bacillus sp. Strain OxB-1. FEMS Microbiology Letters. 158, 185-190

Bak, S., Tax, F. E., Feldmann, K. A., Galbraith, D. W. and Feyereisen, R. (2001) CYP83B1, a Cytochrome P450 at the metabolic branch point in auxin and indole glucosinolate biosynthesis in Arabidopsis. Plant Cell. 13, 101-111

Banerjee, M., Sharma, R. and Bernerjee, U. C. (2002) The nitrile-degrading enzymes: current status and future prospects. Applied Microbial Biotechnology. 60, 33-34

Bauer, R., Knackmuss, H. J. and Stolz, A. (1998) Enantioselective hydration of 2 - arylpropionitriles by a nitrile hydratase from Agrobacterium tumefacies. Applied Microbial Biotechnology. 49, 89-95

Brandao, P. F. B., Clapp, J. P. and Bull, A. T. (2003) Diversity of Nitrile Hydratase and Amidase Enzyme Genes in Rhodococcus erythropolis Recovered from Geographically Distinct Habitats Applied and Environmental Microbiology. 69, 5754–5766

Cameron, R. (2002) Nitrile degrading enzymes from extreme environments. Ph.D thesis. . University of London, London, UK

Cameron, R. A., Sayed, M. and Cowan, D. A. (2005) Molecular analysis of the nitrile catabolism operon of the thermophile Bacillus pallidus RAPc8. Biochimica et Biophysica Acta. 1725, 35–46

Chiyanzu, I. (2008) An investigation into the biocatalytic application of the thermostable nitrile hydratase from the thermophilic strain Geobacillus pallidus RAPc8. Ph.D thesis. . University of Cape Town

Christensen, S., Maenhaut-Michel, G., Mine, N., Gottesman, S., Gerdes, K. and Melderen, L. V. (2004) Overproduction of the Lon protease triggers inhibition of translation in Escherichia coli. Molecular Microbiology. 51, 1705-1717

Colletier, J., Fournier, D., Greenblatt, H. M., Jure, S., Sussman, J. L., Zaccai, G., Silman, I. and Weik, M. (2006) Structural insights into substrate traffic and inhibition in acetylcholinesterase. The EMBO Journal. 25, 2746–2756

Cornish-Bowden, A. (1995) Analysis of Enzyme Kinetic Data. p. 53, Oxford University Press

Cowan, D., Cramp, R., Pereira, R., Graham, D. and Almatawah, Q. (1998) Biochemistry and biotechnology of mesophilic and thermophilic nitrile metabolizing enzymes. Extremophiles. 2, 207-216

Cowan, D. A. (2000) Microbial genomes – the untapped resource. TIBTECH. 18, 14-16

Cowan, D. A., Cameron, R. A. and Tsekoa, T. L. (2003) Comparative biology of mesophilic and thermophillic nitrile hydratases. Advances in Applied Microbiology. 52, 123-153

Cramp, R. A. and Cowan, D. A. (1998) Molecular characterization of a novel thermophilic nitrile hydratase. Biochimica et Biophysica Acta. 1431, 249-260

Dhillon, J., Chhatre, S., Shanker, R. and Shivaraman, N. (1999) Transformation of aliphatic and aromatic nitriles by a nitrilase from Pseudomonas sp. Canadian Journal of Microbiology. 45, 811-815

Duffield, R. M., Shafagati, A., Riddick, E. W., Bowen, S. and Wheeler, J. W. (1990) Mandelonitrile in larval secretion of mountain ash sawfly, Pristiphora geniculata (Hymenoptera: Tenthredinidae). Joural of Chemical ecology. 16, 1103-1110

Endo, I. and Odaka, M. (2000) What evidences were elucidated about photoreactive nitrile hydratase? . Journal of Molecular Catalysis B: Enzymatic 10, 81–86

Endo, T. and Watanabe, I. (1998) Nitrile hydratase of Rhodococcus sp N-774. Purification and amino acid sequences. FEBS Letters. 243, 61-64

Fallon, R. D., Stieglitz, B. and TurnerJr, I. (1997) A Pseudomonasputidacapable of stereoselective hydrolysis of nitriles. Applied Microbiol Biotechnology 47, 156–161

Francisco, I. A. and Pinotti, M. H. P. (2000) Cyanogenic Glycosides in Plants. Brazilian Archives of Biology and Technology. 43, 487-492

Gebicki, J., Sysa-Jedrejowska, A., Adamus, J., Wozniacka, A., Rybak, M. and Zielonka, J. (2003) 1-Methylnicotinamide: a potent anti-inflammatory agent of vitamin origin. Polish Journal of Pharmacology. 55, 109-112

Goda, H., Hashimoto, Y., Shimizu, S. and Kobayashi, M. (2001) Discovery of a novel enzyme, isonitrile hydratase, involved in nitrogen-carbon triple bond cleavage. Journal of Biological Chemistry. 276, 23480-23485

Grodberg, J. and Dunn, J. J. (1988) ompT encodes the Escherichia coli outer membrane protease that cleaves T7 RNA polymerase during purification. Joural of Bacteriology. 170, 1245-1253

Halkier, B. A. and Gershenzon, J. (2006) Biology and biochemistry of glucosinolates. Annual Review in Plant Biology. 57, 303-333

Hannig, G. and Makrides, S. C. (1998) Strategies for optimizing heterologous protein expression in Escherichia coli. Trends in Biotechnology. 2, 54-60

Harper, D. B. (1977) Fungal degradation of aromatic nitriles. Enzymology of C-N cleavage by Fusarium solani. Biochemical Journal. 167, 685-692

Hashimoto, K., Suzuki, H., Taniguchi, K., Noguchi, T., Yohda, M. and Odaka, M. (2008) Catalytic mechanism of nitrile hydratase proposed by time-resolved x-ray crystallography using a novel substrate, tert-butylisonitrile. Journal of Biological Chemistry. 283, 36617-36623

Hashimoto, Y., Hosaka, H., Oinuma, K., Goda, M., Higashibata, H. and Kobayashi, M. (2005) Nitrile pathway involving acyl-CoA synthetase overall metabolic gene organization and purification and characterization of the enzyme. The Journal of Biological Chemistry. 280, 8660-8667

Hensel, M., Lutz-Wahl, S. and Fischer, L. (2002) Stereoselective hydration of (RS)-phenylglycine nitrile by new whole cell biocatalysts. Tetrahedron: Asymmetry. 13, 2629–2633

Holtze, M. S., Sørensen, J., BHansen, H. S. and Aamand, J. (2006) Transformation of the herbicide 2,6-dichlorobenzonitrile to the persistent metabolite 2,6-dichlorobenzamide (BAM) by soil bacteria known to harbour nitrile hydratase or nitrilase. Biodegradation. 17, 503–510

Hourai, S., Miki, M., Takashima, Y., Mitsuda, S. and Yanagi, K. (2003) Crystal structure of nitrile hydratase from a thermophilic Bacillus smithii. Biochemical and Biophysical Research Communications. 312, 340–345

Huang, W., Jia, J., Cummings, J., Nelson, M., Schneider, G. and Lindqvist, Y. (1997) Crystal structure of nitrile hydratase reveals a novel iron centre in a novel fold. Structure. 5, 691-699

Jallageas, J. C., Arnaud, A. and Galzy, P. (1979) Nitrilases and amidases: determination of activity by proton magnetic resonance spectrometry. Analytical Biochemistry. 95, 436–443

Kato, Y. and Asano, Y. (2003) High-level expression of a novel FMN-dependent heme-containing lyase, phenylacetaldoxime dehydratase of Bacillus sp. strain OxB-1, in heterologous hosts. Protein Expression and Purification. 28, 131-139

Kato, Y., Ooi, R. and Asano, Y. (1998) Isolation and characterization of a bacterium possessing a novel aldoxime-dehydration activity and nitrile-degrading enzymes. Archives of Microbiology. 170, 85-90

Kato, Y., Ooi, R. and Asano, Y. (1999a) A new enzymatic method of nitrile synthesis by Rhodococcus sp. strain YH3-3. Journal of Molecular Catalysis B: Enzymatic. 6, 249 – 256

Kato, Y., Ooi, R. and Asano, Y. (2000) Distribution of aldoxime dehydratase in microorganisms. Applied and Environmental Microbiology. 66, 2290-2296

Kato, Y., Tsuda, T. and Asano, Y. (1999b) Nitrile hydratase involved in aldoxime metabolism from Rhodococcus sp. strain YH3-3 Purification and characterization. FEBS Journal. 263, 662-670

Kato, Y., Tsuda, T. and Asano, Y. (2007) Purification and partial characterization of N-hydroxy-L-phenylalanine decarboxylase/oxidase from Bacillus sp. strain OxB-1, an enzyme involved in aldoxime biosynthesis in the "aldoxime–nitrile pathway". Biochimica et Biophysica Acta. 1774, 856–865

Kato, Y., Yoshida, S., Xie, S. X. and Asano, Y. (2004) Aldoxime dehydratase co- existing with nitrile hydratase and amidase in the iron-type nitrile hydratase-producer Rhodococcus sp N-771 . Journal of Bioscience and Bioengineering. 97, 250-259

Kim, S. and Oriel, P. (2000) Cloning and expression of the nitrile hydratase and amidase genes from Bacillus sp. BR449 into Escherichia coli. Enzyme and Microbial Technology. 27, 492–501

Kobayashi, K., Yoshioka, S., Kato, Y., Asano, Y. and Aono, S. (2005) Regulation of Aldoxime Dehydratase Activity by Redox-dependent Change in the Coordination Structure of the Aldoxime-Heme Complex. The Journal of Biological Chemistry. 280, 5486–5490

Kobayashi, M., Nishiyama, M., Nagasawa, T., Horinouchi, S., Beppu, T. and Yamada, H. (1991) Cloning, nucleotide sequence and expression in Escherichia coli of two cobalt-containing nitrile

hydratase genes from Rhodococcus rhodochrous J1. Biochimica et Biophysica Acta (BBA) - Gene Structure and Expression. 1129, 23-33

Komeda, H., Kobayashi, M. and Shimizu, S. (1996) Characterization of the gene-cluster of high-molecular-mass nitrile hydratase (H-NHase) induced by its reaction-product In Rhodococcus-rhodochrous J1. Proc Natl Acad Sci U S A. 93, 4267-4272

Kowlessur, P. (2007) Engineering homoaromatic substrate specificity into aliphatic-specific Geobacillus pallidus RAPc8 Nitrile Hydratase . M.Sc thesis. . University of the Western Cape, Bellville, South Africa

Kuwl, P. W. (1994) Excess-substrate inhibition in enzymology and high-dose inhibition in pharmacology: a re-interpretation. Biochemical Journal. 298, 171-180

Langdahl, B. R., Bisp, P. and Ingvorsen, K. (1996) Nitrile hydrolysis by Rhodococcus erythropolis BLI, an acetonitrile-tolerant strain isolated from a marine sediment. Microbiology. 142, 145-154

Legras, J., Chuzel, A., Arnaud, A. and Galzy, P. (1990) Natural nitriles and their metabolism. World Journal of Microbiology and Biotechnology. 6, 83-108

Li, T., Liu, J., Bai, R., Ohandjad, D. and Wonga, F. (2007) Biodegradation of organonitriles by adapte dactivated sludge consortium with acetonitrile-degrading microorganisms Water Research. 41, 3465–3473

Martinkova, M., Vejvoda, V. and Vladimir, K. (2007) Selection and screening for enzymes of nitrile metabolism. Journal of Biotechnology. 133, 318–326

Mascharak, P. K. (2002) Structural and functional models of nitrile hydratase. Coordination Chemistry Reviews. 225, 201–214

Mauger, J., Nagasawa, T. and Yamada, H. (1988) Synthesis of various aromatic amide derivatives using nitrile hydratase of Rhodococcus rhodochrous J1 Tetrahedron. 45, 1347-1354

Michaelis, L. and Menten, M. (1913) Die kinetik der invertinwirkung. Biochemische Zeitschrift 49, 333-369

Mitra, S. and Holz, R. C. (2007) Unraveling the Catalytic Mechanism of Nitrile Hydratases. The Journal of Biological Chemistry. 282, 7397–7404

Miyanaga, A., Fushinobu, S., Ito, K. and Wakagi, T. (2001) Crystal Structure of Cobalt-Containing Nitrile Hydratase Biochemical and Biophysical Research Communications. 288, 1169 –1174

Mylerová, V. and Martínková, L. (2003) Synthetic Applications of Nitrile-Converting Enzyme. Current Organic Chemistry. 7, 1-17

Nagasawa, T., Nanba, H., Ryuno, K., Takeuchi, K. and Yamada, H. (1987) Nitrile hydratase of Pseudomonas chlororaphis B23. Purification and characterization. European Journal of Biochemistry. 162, 691-698

Nagasawa, T., Takeuchi, K. and Yamada, H. (1991) Characterization of a new cobalt-containing nitrile hydratase purified from urea-induced cells of Rhodococcus rhodochrous J1. European Journal of Biochemistry. 196, 581-589

Nagasawa, T. and Yamada, H. (1989) Microbial transformations of nitriles. Trends in Biotechnology. 7, 153-158

Nagasawa, T. and Yamada, H. (1990) Application of nitrile converting enzymes for the production of useful compounds. Pure and Applied Chermistry. 62, 1441-1444

Odaka, M., Tsujimura, M. and Endo, I. (2001) Post-translational modifications in nitrile hydratase family. RIKEN Review. 41, 58-60

Padmakumar, R. and Oriel, P. (1999) Bioconversion of acrylonitrile to acrylamide using a thermostable nitrile hydratase. Applied Biochemistry and Biotechnology. 77-79, 671-679

Pastrana, L., Gonzalez, M. P., Miron, J. and Murado, M. A. (1998) A new device for measuring diffusional restrictions and modelling substrate inhibition in a starch-glucoamylase system. Biotechnology Letters 20 127–130

Payne, M. S., Wu, S., Fallon, R. D., Tudor, G., Stieglitz, B., TurnerJr, I. M. and Nelson, M. J. (1997) A Stereoselective Cobalt-Containing Nitrile Hydratase Biochemistry. 36, 5447-5454

Peplowski, L., Kubiak, K. and Nowak, W. (2007) Insights into catalytic activity of industrial enzyme Co-nitrile hydratase. Docking studies of nitriles and amides. Journal of Molecular Modelling. 13, 725-730

Pereira, R. A., Graham, D., Rainey, F. A. and Cowan, D. A. (1998) A novel thermostable nitrile hydratase. Extremophiles. 2, 347-357

Prepechalová, I., Martínková, L., Stolz, A., Ovesná, M., Bezouska, K., Kopecky, J. and Kren, V. (2000) Purification and characterization of the enantioselective nitrile hydratase fromRhodococcus equiA4. Applied Microbial Biotechnology. 55, 150-156

Raj, J., Prasad, S. and Bhalla, T. C. (2006) Rhodococcus rhodochrous PA-34: A potential biocatalyst for acrylamide synthesis. Process Biochemistry. 41, 1359–1363

Reisinger, C., Osprian, I., Glieder, A., Schoemaker, H. E., Griengl, H. and Schwab, H. (2004) Enzymatic hydrolysis of cyanohydrins with recombinant nitrile hydratase and amidase from Rhodococcus erythropolis. Biotechnology Letters. 26, 1675–1680

Rodionov, D. A., Hebbeln, P., Gelfand, M. S. and Eitinger, T. (2006) Comparative and Functional Genomic Analysis of Prokaryotic Nickel and Cobalt Uptake Transporters: Evidence for a Novel Group of ATP-Binding Cassette Transporters. Journal of Bacteriology. 188, 317–327

Rustler, S. and Stolz, A. (2007) Isolation and characterization of a nitrile hydrolysing acidotolerant black yeast—Exophiala oligosperma R1. Applied Microbial Biotechnology. 75, 899–908

Shi, J., Blundell, T. L. and Mizuguchi, K. (2001) FUGUE; Sequence-structure homology recorgnition using environmental specific substitution tables and structure-dependent gap penalties. Journal of Molecular Biology. 310, 243-257

Song, L., Wang, M., Shi, J., Xue, Z., Wang, M. and Qian, S. (2007) High resolution X-ray molecular structure of the nitrile hydratase from Rhodococcus erythropolis AJ270 reveals posttranslational oxidation of two cysteines into sulfinic acids and a novel biocatalytic nitrile hydration mechanism. Biochemical and Biophysical Research Communications. 362, 319-324

Stevens, J. M., Saroja, N. R., Jaouen, M., Belghazi, M., Schmitter, J., Mansuy, D., Artaud, I. and Sari, M. (2002) Chaperone-assisted expression, purification, and characterization of recombinant nitrile hydratase NI1 from Comamonas testosteroni. Protein Expression and Purification. 29, 70-76

Stolz, A., Trott, S., Binder, M., Bauer, R., Hirrlinger, B., Layh, N. and Knackmuss, N. (1997) Enantioselective nitrile hydratases and amidases from different bacterial isolates. Journal of Molecular Catalysis B: Enzymatic. 5, 137-141

Stowe, B. B. and Hudson, V. W. (1969) Growth Promotion in Pea Stem Sections. III. By Alkyl Nitriles, Alkyl Acetylenes and Insect Juvenile Hormones. Plant Physiology. 44, 1051-1057

Takashima, Y., Yamaga, Y. and Mitsuda, S. (1998) Nitrile hydratase from a thermophilic Bacillus smithii. Journal of Industrial Microbiology & Biotechnology. 20, 220-226

Tani, O., Kurihara, M. and Nishise, H. (1989) Characterization of Nitrile Hydratase and Amidase, Which Are Responsible for the Conversion of Dinitriles to Mononitriles, from Corynebacterium sp. Agricatural Biological Chemistry. 53, 3151-3158

Thimann, K. V. and Mahadevan, S. (1964) Nitrilase. I. occurrence, preparation, and general properties of the enzyme. Archives of Biochemistry and Biophysics. 105, 133-141

Thomas, S. M., DiCosimo, R. and Nagarajan, A. (2002) Biocatalysis: applications and potentials for the chemical industry. Trends in Biotechnology. 20, 238-242

Thomsen, R. and Christensen, M. H. (2006) MolDock: A new technique for high-accuracy molecular docking. Journal of Medical Chemistry. 49, 3315-3321

Tsekoa, T. L. (2005) Structure, enzymology and genetic engineering of Bacillus sp. RARc8 Nitrile Hydratase. Ph.D thesis. University of the Western Cape, Bellville, South Africa

Vino, S. and Lokesh, K. R. (2008) Borrelidin: A promising anticancer agent from Streptomyces species. Advanced Biotechnology. 6, 22-26

Wang, M. (2005) Enantioselective Biotransformations of nitriles in organic synthesis. Topics in Catalysis. 35, 117-131

Wieser, M., Takeuchi, K., Wada, Y., Yamada, H. and Nagasawa, T. (1998) Low-molecular-mass nitrile hydratase from Rhodococcus rhodochrous J1: purification, substrate specificity and comparison with the analogous high-molecular–mass enzyme. FEMS Microbiology Letters. 169, 17-22

Woodward, A. and Bartel, B. (2005) Auxin: Regulation, action and interaction Annals of Botany. 95, 707–735

Wyatt, J. M. and Knowles, C. J. (1995) Microbial degradation of acrylonitrile waste effluents: the degradation of effluents and condensates from the manufacture of acrylonitrile. International Biodeterioration & Biodegradation, 221-248

Wyatt, J. M. and Knowles, C. J. (1995) The development of a novel strategy for the microbial treatment of acrylonitrile effluents. Biodegradation. 6, 93–107

Yamada, H. and Kobayash, M. (1996) Nitrile hydratase and its application to industrial production of acrylamide. Bioscience Biotechnology and Biochemistry. 60, 1391-1400

Yamaki, T., Oikawa, T., Ito, K. and Nakamura, T. (1997) Cloning and sequencing of a nitrile hydratase gene from Pseudonocardia thermophila JCM3095. Journal of Fermention Bioengineering. 83, 474-477

Yamamoto, K., Ueno, Y., Otsubo, K., Yamane, H., Komatsu, K. and Tani, Y. (1992) Efficient conversion of dinitrile to mononitrile-monocarboxylic acid by Corynebacterium sp. C5 cells during tranexamic acid synthesis. Journal of Fermentation and Bioengineering. 73, 125-129

Yeom, S., Kim, H. and Oh, D. (2007) Enantioselective production of 2,2-dimethylcyclopropane carboxylic acid from 2,2-dimethylcyclopropane carbonitrile using the nitrile hydratase and amidase of Rhodococcus erythropolis ATCC 25544. Enzyme and Microbial Technology 41 842–848

Appendices

Appendix 1 Ammonium sulphate fractionation

	Final concentration of ammonium sulphate, % saturation																
	10	20	25	30	33	35	40	45	50	55	60	65	70	75	80	90	100
	Grams solid ammonium sulphate to be added to 1L. of solution																
0	56	114	144	176	196	209	243	277	313	351	390	430	472	516	561	662	767
10		57	86	118	137	150	183	216	251	288	326	365	406	449	494	592	694
20			29	59	78	91	123	155	189	225	262	300	340	382	424	520	619
25				30	49	61	93	125	158	193	230	267	307	348	390	485	583
30					19	30	62	94	127	162	198	235	273	314	356	449	546
33						12	43	74	107	142	177	214	252	292	333	426	522
35							31	63	94	129	164	200	238	278	319	411	506
40								31	63	97	132	168	205	245	285	375	469
45									32	65	99	134	171	210	250	339	431
50										33	66	101	137	176	214	302	392
55											33	67	103	141	179	264	353
60												34	69	105	143	227	314
65													34	70	107	190	275
70														35	72	153	237
75															36	115	198
80																77	157
90																	79

Appendix 2 Biorad Bradford assay standard curve

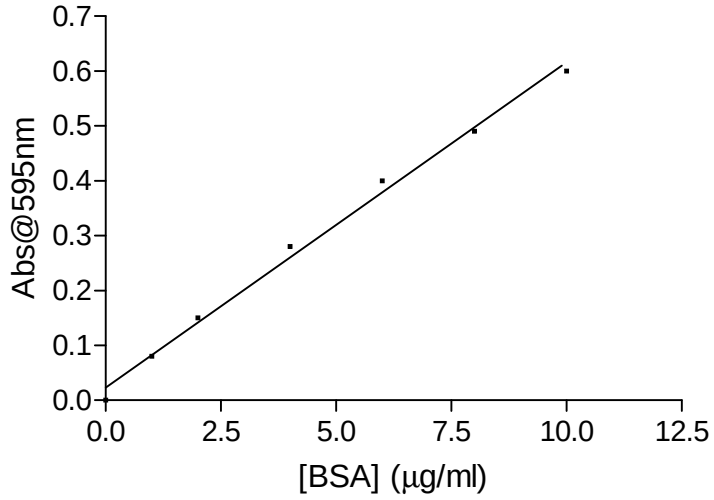

$y = 0.059x + 0.023$

$R^2 = 0.994$

Appendix 3 Ammonia assay standard curve

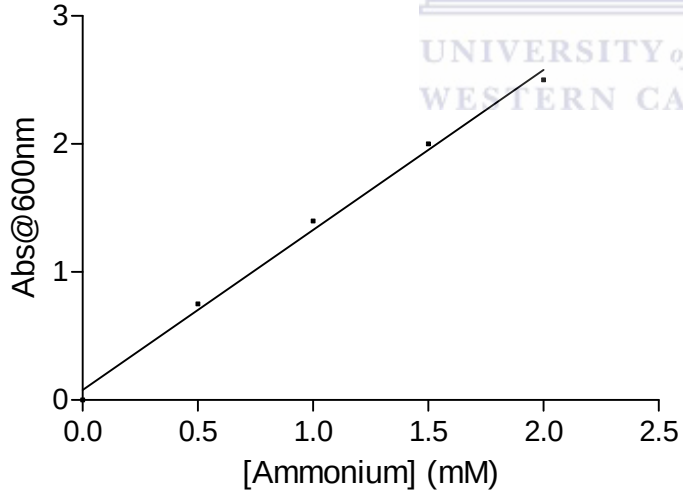

$y = 1.25x + 0.080$

$R^2 = 0.9945$

UNIVERSITY of the
WESTERN CAPE